Nanofluidic System for Single Molecule Manipulation and Analysis

By

Yi-Heng Sen

B.S. Electrical Engineering
National Taiwan University, 2004

Submitted to the Department of Mechanical Engineering
in Partial Fulfillment of the Requirement for the Degree of

Master of Science in Mechanical Engineering

at the

Massachusetts Institute of Technology

September 2008

Signature of Author: _____
Department of Mechanical Engineering
August 14th, 2008

Certified by: _____
Rohit N. Karnik
Assistant Professor of Mechanical Engineering
Thesis Advisor

Accepted by: _____
Lallit Anand
Professor of Mechanical Engineering
Chair, Departmental Committee on Graduate Students

Nanofluidic System for Single Molecule Manipulation and Analysis

By

Yi-Heng Sen

Submitted to the Department of Mechanical Engineering
on August 14th, 2008 in partial fulfillment of the
requirement for the Degree of Master of Science in
Mechanical Engineering

Abstract

This thesis focuses on characterizing and controlling the translocation of single 48.5 kbp λ-DNA molecules through an artificial nanopore with the objective of enabling multiple measurements on the same molecule. This approach may enable nanopore sensors with enhanced size or charge resolution through statistical averaging over multiple detection events. Nanopores with dimensions of 200 nm × 500 nm × 5 μm connected by microfluidic channels were fabricated using soft lithography in polydimethylsiloxane (PDMS). The PDMS nanopore could successfully detect translocation events of single λ-DNA molecules. Factors such as applied voltage bias, DNA concentration, and dimensions of the channel were found to affect the frequency of translocation events and signal-to-noise ratio, which are critical factors for implementing multiple measurements on the same molecule with feedback control. Noise contributions from each part of the experimental apparatus and device were also characterized. Feedback control using Labview was implemented to reverse the direction of applied voltage bias upon detection of a translocation event. The direction of travel of single DNA molecules could be successfully reversed and two measurements on the same molecule were realized. This work lays the foundations for a nanofluidic device for enhanced measurement resolution through statistical averaging over multiple measurements on the same molecule.

Thesis Supervisor: Rohit N. Karnik

Title: Assistant Professor of Mechanical Engineering

Acknowledgements

First of all, I owe numerous thanks to my advisor, Professor Rohit Karnik, for his guidance, encouragement, patience, intellectual wisdom, and professional support. He is one of the nicest people to have as an advisor, and I deeply appreciate him introducing me to the lab. Without this opportunity, I would not have finished my masters degree at MIT!

I would like to thank all of my group members, Suman Bose, Pedro Valencia, Pamela Basto, Mohamed Raafat, Chia-Hua Lee, and Dorothy Hanna, for their help and friendship. I am grateful to work together with them. I would like to thank Professor Ali Khademhosseini, who offered me the teaching assistantship last spring. I would like to thank Hsiao-Wei, who motivates me to be a better person. I would like to thank my friends at MIT, who have made my graduate life colorful. I would like to thank my friends in Taiwan for their friendship and support.

I would like to thank MIT Aeronautical/Astronautical department (Marie Stuppard and Barbara Lechner), Mechanical Engineering department (Leslie Regan and Joan Kravit), Microsystems Technology of Laboratories (Dr. Vicky Diadiuk, Kurt Broderick, David Terry, Paul Tierney, Paudely Zamora, and Dennis Ward,) and Research Laboratories of Electronics (Mark Mondol).

Finally, I would like to express my deepest appreciation to my parents and sister for their love and support. No words are sufficient to thank them here!

Table of Contents

List of Figures

List of Tables

Chapter 1 Introduction

1.1 Background

Rapid and sensitive analysis of biomolecules is central to several fields such as molecular biology, medical diagnostics, and biotechnology. Detection and analysis techniques can be broadly classified into techniques based on physical or biochemical characteristics of the analyte, and techniques that use biological recognition and labeling with antibodies or other molecules for analysis. Label-based techniques are typically very specific for the detection of molecules, organelles, or cells in a high background of other materials and are extremely useful research tools in conjunction with microscopy. However, they typically require extensive processing steps and development of antibodies or other recognition elements, and are usually not optimal for rapid and quantitative analysis of biological macromolecules and particles when information about physicochemical characteristics such as size or charge is required. Such applications include sizing of cell suspensions, analysis of the lengths of products of polymerase chain reactions or restriction digestion, or examining the morphology of cells.

While rapid analysis of cells is easily carried out using cytometers[1] and Coulter counters, efforts have been directed towards miniaturization of these devices to the nanoscale. With advances in micro and nanofabrication technology, miniaturization of Coulter counters have successfully detected and sized viruses, nanoparticles, and protein complexes[2-5]. The ultimate limit of miniaturization of these sensors has resulted in nanopores for rapid, label-free analysis of single biomolecules[2, 6-12]. Nanopores rely on resistive pulse sensing in which current through the a pore changes during translocation

(passage) of a molecule through the pore, very similar to the working principle of the Coulter counter (Figure 1)[11].

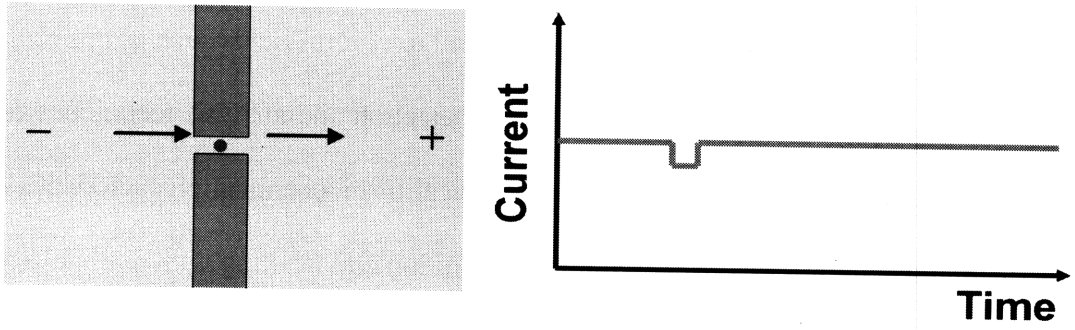

Figure 1 A nanopore detects a particle by change in current during translocation.

Most efforts to develop nanopore technology have been directed at DNA sequencing using α-hemolysin nanopores or artificial nanopores with diameters in the 1-10 nm size range[6, 13-15], with some efforts directed at analysis of larger molecules, colloids, and particles[3, 4, 16]. Nanopores for DNA sequencing research have very small size that enables close molecular interactions between the DNA molecule and the nanopore, and therefore can be used to extract molecular-level information about the analyte[17]. However, nanopores that are tailor-made for detection of DNA are typically not suitable for detection of larger molecules of unknown or varying size, which requires larger pore size and the ability to detect and analyze particles that may be considerably smaller than the pore cross-section. Several biologically important analytes such as fragments of genomic DNA, viruses, large proteins and protein complexes, and cell organelles lie in this size range of 10-500 nm.

1.2 Nanopore Sensor Devices

1.2.1: Protein nanopores

The protein nanopore formed by α-haemolysin (αHL) from Staphylococcus aureus has become a model system for prospective analytical applications because it can be tricked into remaining fully open for a long period of time[18]. In 1996, Kasianowicz et al.[6] demonstrated that the translocation of single DNA molecules through the naturally occurring hemolysin pore could be detected by monitoring the ionic current through the pore. These nanopores self-assemble from subunits into a lipid bilayer membrane. The diameter of the larger opening of the resulting nanopore is 2.6 nm while that of the smaller opening is about 1.5 nm. As the DNA molecule passes through the pore, it sterically blocks the pore, resulting in a transient decrease in the ionic current through the pore. The remarkable success of α-hemolysin may be attributed to its stability and a size that is just larger than a single stranded DNA molecule, enabling close molecular interactions between the DNA molecule and the nanopore during translocation. Howorka and Bayley[7] engineered this pore and attached a short DNA strand inside the pore. By measuring the translocation time and current blockages of DNA strands of different lengths with a sequence complementary to the covalently attached segment, they were able to infer the electrical potential distribution along the length of the pore. Hemolysin pores could discriminate between current blockages due to purine and pyrimidine segments in a DNA molecule, showing promise for rapid DNA sequencing[19]. Meller et al.[13] demonstrated the potential of hemolysin pores to characterize molecules by discriminating between polynucleotides with similar length and composition, but differing only in sequence. Bates et al.[20] studied DNA polymer biophysics by driving DNA molecules into the hemolysin pore and switching off the driving voltage using feedback control and subsequently looking at escape times of DNA molecules from an

entropically unfavorable configuration. Wang et al.[21] further characterized DNA samples and demonstrated that modifications such as phosphorylation result in different statistical signatures of DNA molecules translocating through hemolysin pores (Figure 2).

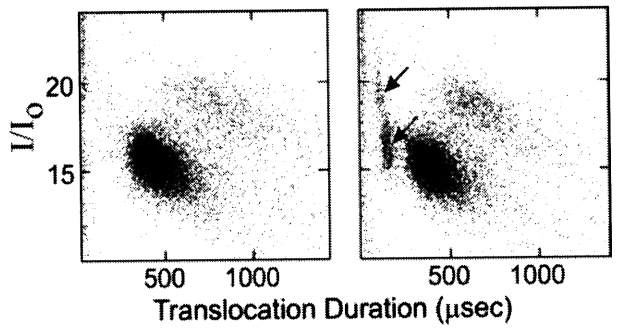

Figure 2 Current change and translocation duration profiles can be used to distinguish between a sample with 100-base DNA with only the base A (a) and a mixture of 100-base DNA with only A and a minor component of 100-base DNA with only C (arrows).(b) Reproduced from Wang et al.[21]

1.2.2 Solid-state nanopores

While protein channels offer a well-defined geometry and are amenable to bio-chemical modification, it is difficult to change the pore size, and they are not amenable to integration with upstream or downstream processing. These drawbacks resulted in the search for methods to fabricate artificial nanopores that are more robust and give control over nanopore geometry. Li et al.[8] introduced the method of ion-beam sculpting, in which a 1.8 nm diameter nanopore could be fashioned in a silicon nitride membrane using the bombardment of argon ions to slowly close a larger pore by redistribution of material around the pore. Storm et al.[10] demonstrated controlled size reduction of a pore

in silicon dioxide using a high energy TEM to fluidize the glass and shrink it due to surface tension. The TEM allowed monitoring of the process and the pore diameter could be controlled down to one nanometer precision. Chang et al.[14] fabricated a 50-60 nm long, 4-5 nm diameter pore using e-beam and standard lithography techniques for DNA sensing. Smeets et al.[22] studied the dependence of current fluctuations on electrolyte concentration during DNA translocation through solid state nanopores. Siwy et al.[23] fabricated a conical nanopore using ion track etching technique. This pore also exhibited a voltage-dependent switching characteristic, similar to biological voltage-gated channels. These pores were also functionalized with molecular binding agents such as biotin and antibodies and were shown to be capable of highly specific molecule detection[24]. Harrell et al.[25] deposited gold inside conical nanopores for functionalization with thiolated DNA molecules. Due to their charge, DNA molecules responded to applied electric potentials by changing their conformation, resulting in current rectification.

Nanopores designed for the sequencing of single DNA molecules need to have small diameters (<10 nm) to ensure adequate signal. There is a trade-off in terms of dynamic range, and it is difficult to analyze larger proteins, molecules, or particles of unknown or varying sizes using nanopores tailor-made for analysis of oligonucleotides. A few research groups have targeted analysis of particles and colloids in the submicron size range in miniaturized Coulter counter type systems[2-5]. In contrast to nanopores that are sufficiently small to ensure molecular-level interactions that have the potential to yield structural information about the molecule, larger pores are more suitable for determining the physicochemical characteristics of molecules and particles such as size and charge[26]. It may be envisaged that nanopores with different surfaces such as hydrophilic,

hydrophobic, aromatic, or charged, may be used to gain additional information about the molecule or particle of interest. Sizing of several viruses using a 400 nm pore was accomplished as early as 1977 by DeBlois and Wesley[27]. Using monodisperse solutions of viruses, they were able to characterize the size of each type of virus within a few nanometers. Recently, Saleh and Sohn[16] used rapid prototyping in PDMS and glass etching to make 200-400 nm nanopores. They have demonstrated detection of λ-DNA[16], 87 nm latex colloids[4], and later used this system for detection of protein binding to colloidal nanoparticles for binding assays[3]. The nanopore was used for the detection of human granulocyte colony stimulating factor and granulocyte and macrophage colony stimulating factor[28]. Sridhar et al. detected particles that have volume ratio to the sensing channel as low as 0.006% by using a MOSFET-based Coulter counter[29]. Other researchers have detected single DNA molecules and nanoparticles using nanopipettes[5]. Ito et al used a carbon nanotube pore to determine the size and surface charge of nanoparticles in the 60 nm size range[26]. Uram et al used 500-600 nm diameter laser machined pores for detection and sizing of virus particles and to determine the number of antibodies bound to virus particles[30], and for detection of staphylococcal enterotoxin B by sensing the translocations of immune complexes through the pore[31].

1.3 Mechanism of Current Change and Noise Characterization

1.3.1: Mechanism of current change

While current change in a typical Coulter counter results from blockage of the pore leading to a decrease in current, charges on the analyte or on the surface play an important role in nanofluidic transport[32-34]. Researchers have reported both current

decrease as well as current increase[14] during translocation of DNA through nanopores. Fan et al. have demonstrated that at low ionic concentrations, the charge on the DNA molecule can dominate ionic current through the nanopore by introducing mobile counterions into the pore[34]. Karnik et al. have demonstrated that the same principle applies in the case of protein binding inside nanochannels, leading to increase in current at low ionic concentrations, and decrease in current due to blockage at high ionic concentrations[33]. Furthermore, the effect of charge on the biomolecule almost exactly cancels the blockage effect due to its size at ionic concentrations equal to the charge to volume ratio of the molecule[33]. Current decreases during translocation of DNA at concentrations of approximately 0.5 M or higher, but increases at lower concentrations[34]. By proper choice of the buffer ionic concentration, analytes can be sensed either via their charge effect or via their size effect. This phenomenon has also been studied and observed in 10 nm artificial nanopores[22].

1.3.2 Noise in resistive-pulse sensing

As the size of the analyte is decreased, noise levels increase and discrimination between particles or molecules with slight differences in size becomes more difficult. This problem is well-known to researchers in the field of nanopore sensors, and several approaches to improve signal have been proposed. These methods include use of transverse or oscillating electric fields[35], surface modification[36], and optical tweezers[37]. Relatively few studies are directed at understanding the origins of noise in nanopores, and the noise characteristics seem to originate due to different phenomena in different systems. For example, noise in ion track-etched polymer membrane nanopores was

found to occur due to opening and closing of the membrane pore[38], while that in solid-state silica nanopores was found to occur due to nanobubbles[39]. Other researchers have reported decrease in noise upon surface modification of the pore[36]. Noise in membrane pores arising due to dielectric capacitance could be reduced by coating the membrane with PDMS[40]. Very recently, Smeets et al characterized the noise in artificial silicon nitride and oxide nanopores and found two different regimes of noise[15]: 1/f flicker noise that depended on the number of charge carriers dominated at frequencies lower than 100 Hz, while Johnson noise due to dielectric capacitance of the membrane dominated at frequencies above 1 kHz. However, the noise characteristics varied strongly between different pores[15]. Recently, Uram et al discussed theoretically and experimentally how the signal bandwidth and noise of current recordings from individual submicrometer pores or nanopores can critically affect the sensitivity, accuracy, and information content from resistive-pulse sensing experiments[41]. A second source of uncertainty in measurements arises from the different configurations or conformations of a particle or molecule as it passes through the pore. For example, DNA molecules can fold during translocation, and the current blockage duration due to translocating nanoparticles can be affected by the radial position of the particle in the pore[42]. It is more difficult to control this uncertainty, as it would require control over how the molecule or particle translocates through the pore.

1.4. New Approach to Enhance Resolution of Nanopore Sensor

As the size of the analyte decreases below the micrometer length scale, measurement noise increases, making it difficult to distinguish between translocation events of analytes

with only slight differences in size. This poor signal-to-noise ratio is widely recognized as a problem that arises in part due to insufficient measurement time during translocation[19, 37]. In existing designs of nanopores and Coulter counters, the analyte particle or molecule escapes into the solution after a single measurement, limiting the time during which the particle is analyzed. However, if multiple (N) measurements were possible on the same particle for the duration of translocation event and its magnitude of current change, the signal-to-noise ratio may be expected to be dramatically enhanced and the spread in the distributions would be decreased as $N^{0.5}$, permitting the use of such nanopores as sensitive probes for label-free analysis of nanoscale particles and molecules[43, 44] (Figure 3 and 4).

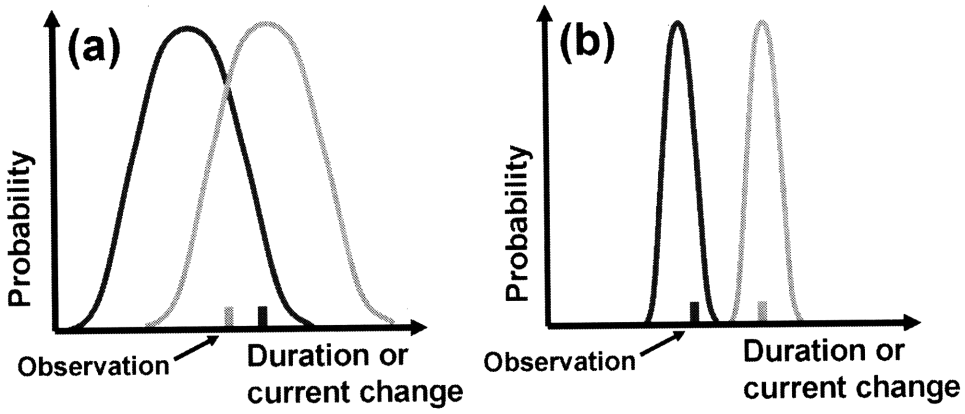

Figure 3 Cartoon to illustrate the efficacy of multiple measurements. (a) Single translocation event distributions for two different types of molecules (light and dark lines) may exhibit significant overlap. Observation of a single event is insufficient to distinguish between the two molecules. (b) Distributions of events consisting of multiple translocations will be narrower. Since overlap of translocation event distributions for two different types of molecules significantly decrease, observation of a single event

(consisting of multiple translocations of a single molecule) is now sufficient to distinguish between the two molecules.

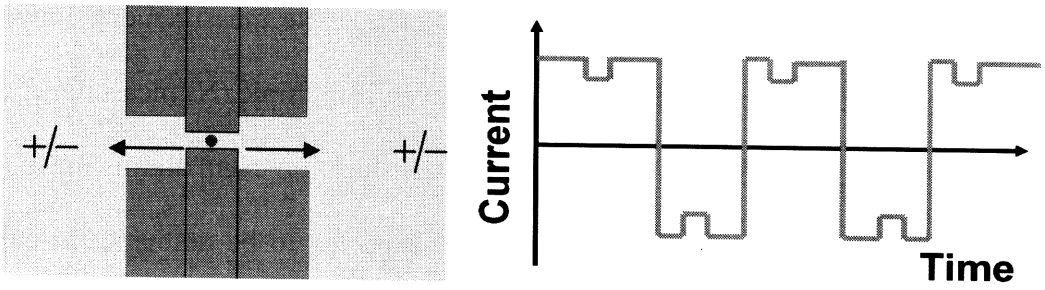

Figure 4 Concept of a device in which multiple translocation events may be recorded for each particle using a nanofluidic system with feedback control, greatly enhancing the resolution of the measurement.

In this thesis, we envisioned a system in which the same molecule could be transported through a nanopore multiple times by implementing feedback control. Specifically, we envisioned a nanofluidic system consisting of a nanopore flanked by two nanofluidic reservoirs that serve to trap analytes (Figure 4). Upon detection of a translocation signal, the applied voltage bias may be reversed, forcing the particle or molecule back into the nanopore. For proof of concept, 48.5 kbp λ-DNA was used as analyte since it had been detected in larger sized nanopores[16]. Soft-lithography was adopted because of its ease of fabrication and capability to fabricate nanopore reservoirs. Moreover, since the success of multiple measurements on the same molecule depends on factors such as translocation rate, length of time interval between translocation events, and noise of the signals, we characterized (a) how the magnitude of applied voltage, buffer solution concentration, and analyte concentration affects the rate and inter-arrival time of the analyte passing

through the nanopore., and (b) how factors such as electronic equipments, measurement setup, magnitude of applied voltage and buffer solution concentration contribute to the noise of the system.

1.5 Thesis Overview

In this thesis, we focus on characterizing and controlling the translocation of single λ-DNA molecule through an artificial PDMS nanopore with the objective of enabling multiple measurements on the same molecule. The rest of the thesis is organized as follows. Chapter 2 describes the design and fabrication of the PDMS nanopore devices, and the experimental setup for the measurement. Chapter 3 characterizes the current signals of the DNA passage through the PDMS nanopore, and the corresponding theory of these current pulses. We also characterize the noise of current signals in this PDMS nanopore system. Chapter 4 describes the experimental setup and implementation of feedback control that enables multiple measurements on the same molecule. In addition, it describes the corresponding experimental data of two measurements on the same molecule. The last chapter covers the ongoing work, and suggestions for future directions and work to enhance the performance and capabilities of our nanopore-nanofluidic system.

Chapter 2 Design and fabrication of nanopore sensor device

2.1 Introduction

There are mainly two types of nanopores, i.e., α-hemolysin nanopores and solid state nanopores. As we have discussed earlier, solid state nanopores have advantages over α-hemolysin nanopores in that it is easy to control pore size of the solid state nanopores. Moreover, solid state nanopores are amenable to integration with upstream or downstream processing, and are able to withstand a wide range of analyte solutions and harsh chemical environments.

Below we will first describe the design considerations for both fabrication process as well as the dimensions of our solid-state nanopore device. Afterwards, we will give an overview of the designed fabrication process, the equipments used for fabrication, and details of the fabrication. Last, we will discuss issues encountered during fabrication.

2.2 Fabrication of Nanopore Device

2.2.1 Design considerations for fabrication process

Below are design considerations of choosing fabrication process:

1. Ability to fabricate nanofluidic reservoirs on either side of nanopore.
2. Simplicity, reproducibility, and ease of manufacture.
3. Ability to chemically modify the surface.
4. Ability to accurately control ionic concentration without problems such as evaporation.
5. Length commensurate with diffusion timescales of chemical and biological species to facilitate rinsing and reactions.
6. Ability to detect long λ-DNA molecules.

There are several techniques for fabricating nanopores with diameters ranging from ~0.25 nm to 10 nm. Such techniques include the use of atomic-layer-deposition[36]drilling with transmission-electron-microscope (TEM)[10, 45-47] or focused-ion-beam[8, 45, 48, 49], and ion-tracks etching[11, 50, 51]. However, these methods result in a nanopore in a membrane, and are not suitable for incorporation nanofluidic reservoirs for trapping analyte at either side of the nanopore. Moreover, they are difficult to scale up, as they require fabrication of one nanopore at a time.

Fabrication process of using (1) soft-lithography for PDMS nanopore, and (2) anodic boding or sacrificial layer etching techniques for fabricating silica nanopore could both incorporate nanofluidic reservoirs. Process of fabricating silica nanopore had been considered. However, this technique is expensive, and fabrication process is more complicated and time consuming than that using soft lithography. We therefore adopted soft-lithography for fabricating nanopore devices. Soft lithography represents a non-photolithographic strategy that provides a convenient, effective, and low-cost method for manufacturing of micro- and nanostructures[52]. More importantly, soft-lithography process is capable of fabricating nanofluid traps on either side of the nanopore. The geometry of the nanofluidic trap could be designed such that it has significant electric field around both ends of the nanopore, and therefore the rate of recapture would be potentially higher then that without such traps. While fabrication of extremely small nanopores may not be feasible with PDMS (poly-dimethysiloxane, Sylgard 184 elastomer, K.R. Anderson), it has been reported[16] that nanopores in the 150-300 nm range are adequate for analyzing long 48.5 kbp λ-DNA, which is sufficient for proof-of-concept.

2.2.2 Design considerations for nanopore device dimension

For the length of the nanopore, it is shown that shorter nanopore leads to larger electric field at the entrance of the nanopore, and therefore the chances of DNA molecules entering the nanopore would be higher[53]. Here we chose the length of the nanopore to be 5 μm because it is the maximum resolution a transparency mask can reach.

The width of the nanopore should be as small as possible since smaller nanopore leads to less chances of having multiple DNA entering the nanopore at the same time. In addition, DNA translocation signals are more detectable in a smaller nanopore. Here we chose 200 nm for the width since so far it is the minimum width of the metal line we could pattern.

The height of the nanopore should also be as small as possible for the same reason as that for the width. It has been reported that a height of ~78 nm has been achieved in PDMS nanopore without collapse[54]. However, such height could be achieved with certain special fabrication process, which we would not use in our work. We chose 200 nm for the height in this thesis since it has been reported that for PDMS ~150 nm is the minimum achievable pore diameter of PDMS (Sylgard 184) with simple replica molding technique of soft-lithography[16].

For the dimension of the microchannel, we chose the width to be 1 mm and the height to be 10 μm such that it would have significantly lower resistance than that passing of the nanopore.

2.2.3 Overview of the fabrication process

We first fabricated the master mold defining the configuration of the nanopore device. Subsequently we fabricated PDMS nanopore from the master mold, and bonded it to a glass slide to yield nanopore devices. The master mold was fabricated on a silicon wafer using e-beam lithography to pattern titanium (Ti) metal lines that defined the nanopore. Ti lines were patterned using the lift-off technique with a thickness of 200 nm, widths ranging from 200-500 nm, and lengths ranging from 5-8 μm. Subsequently, 10 μm thick SU-8 photoresist was patterned on the silicon wafer to define connecting microfluidic channels. This two-step procedure resulted in a master mold with metal lines defining nanochannels and SU-8 epoxy defining the microfluidic channels. To aid removal of PDMS from the mold, the wafer was placed in a desiccator with a few drops of tridecafluoro-1,1,2,2-tetrahydrooctyl-1-trichlorosilane (United Chemical Technologies). PDMS monomer and curing agent were mixed with usual 10:1 ratio and poured on the mold. The device was cured for 2 days at 80 °C, removed from the mold, punched for input/output ports, cleaned with ethanol and isopropanol (IPA), and bonded to a clean glass slide using oxygen plasma to result in a nanopore device. Figure 5 shows a schematic of the fabrication process of PDMS nanopore device used in the following chapters.

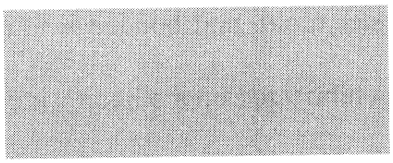

a) Start with silicon wafer

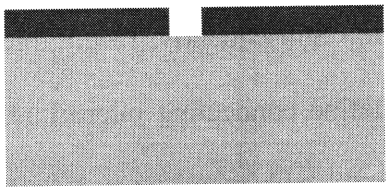

b) Pattern 300 nm PMMA

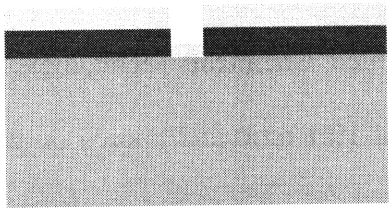

c) Evaporate 200 nm Ti

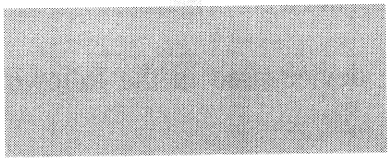

d) Lift-off to have metal line

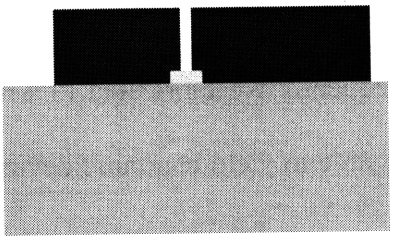

e) Pattern 10 μm of SU-8

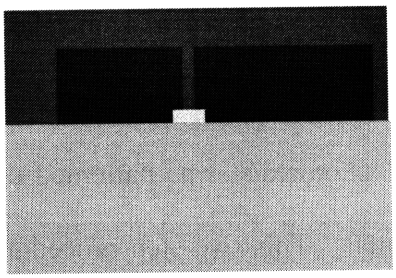

f) Pour PDMS on the mold

g) Release and punch PDMS

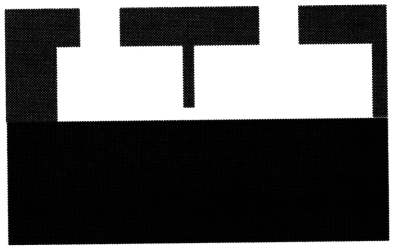

h) Bond to a glass slide

Figure 5 Schematic fabrication process of PDMS nanopore device.

2.2.4 Equipment used in the fabrication process

The master mold was fabricated in Massachusetts Institute of Technology (MIT)'s Microsystem Technology Laboratory (MTL) and the Scanning-Electron-Beam Lithography (SEBL) at the Research Laboratory of Electronics (RLE). Soft-lithography

was done in our laboratory. Table 1 below lists various equipments used in the process, with a "machine coral name" by which they are known in the MTL and RLE at MIT, and a brief description.

Table 2.1 List of MTL and RLE's equipment used in the fabrication process for master mold.

Machine name	Description
Raith 150	Scanning electron beam lithography
Photo-wet	Photo-wet station for develop, lift-off, and rinsing process
PMMA spinner	Manual photoresist spinner specifically for PMMA
EbeamFP	E-beam evaporator
EV1	4" and 6" UV lithography system
SU8spinner	Manual photoresist spinner specifically for SU-8
Asher	Plasma system with Air, O_2

2.2.5 Fabrication of the master mold

A 4" silicon wafer was used as substrate for the master. A positive photoresist PMMA 950 A4 (polymethyl methacrylate, Microchem corporation) with 4% solid content in anisole was spun at 500 rpm for 5 s, and at 1500 rpm for 45 s to yield a film of 300 nm thickness. Following this step, the wafer was softbaked at 180 °C for 8 min to harden the photoresist. Following this step, PMMA was patterned using e-beam lithography to define the configuration of the nanopore. Since the length of the nanopore is defined by

the spacing between the two SU-8 micro channels, the patterned length was chosen to be 100 μm to ensure the connection between two SU-8 microchannels. The width of nanopore was chosen to be 200 nm and 500 nm for the reasons stated in previous section. The dose factor for e-beam lithography was 70 $\mu A/cm^2$ to 90 $\mu A/cm^2$, and the electron-beam energy was 10 keV. PMMA was developed in MIBK/IPA 1:2 ratio (volume) at 21 °C. Since the mixing between MIBK and IPA is an endothermic process, it took ~ 3 hours to develop the PMMA after MIBK and IPA were mixed. Subsequently, the wafer was deposited with 200 nm of titanium (Ti) using e-beam evaporation. The thickness of Ti defined the height of the PDMS nanopore. Ti was chosen for its good adhesion to the silicon wafer. Subsequently, the wafer was submerged in acetone for 2.5 hours for lift-off, followed by rinsing with IPA and drying by nitrogen. Following this step, the substrate was cleaned with air plasma for 1 min, followed by 5 min of baking at 150 °C for dehydration. Without these two steps, the SU-8 would peel off from the substrate once developed. Negative photoresist SU-8 2007 was spun for 5 s at 500 rpm, and 1500 rpm for 40 s more to have a thickness of 10 μm. Following this step, the wafer was soft baked at 65 ° C for 1 min and 95 ° C for 3 more min. Gradual heating was necessary in both soft bake and hard bake to prevent the SU-8 from peeling off the substrate. Subsequently, the wafer was aligned and exposed with UV light at 10 mW/cm^2 for 13 s. Following this step, the wafer was hard baked to 95 °C for 4 min, and cooled down to 45 °C. Following this step, the pattern was developed with ethyl lactate for 3 min, followed by rinsing with IPA, and drying with nitrogen. Subsequently, the wafer was hard baked to 150 °C gradually for 6 min to eliminate cracks in SU-8. Following this step, the master was ready for soft-lithography.

2.2.6 Soft-lithography for the PDMS nanopore device

Nanopore devices were fabricated using soft lithography in poly(dimethysiloxane) (PDMS)[55] in our laboratory. Soft lithography enables rapid fabrication of devices once a master mold is fabricated. To aid removal of PDMS from the mold, the wafer was placed in a dessiccator with a few drops of tridecafluoro-1,1,2,2-tetrahydrooctyl-1-trichlorosilane (United Chemical Technologies). PDMS monomer and curing agent were mixed with the usual 10:1 ratio and poured on the mold. The curing time and temperature are two critical factors that determine whether PDMS nanopore would collapse. Here PDMS device was cured at 80 °C for 2 days and removed from the mold. We punched two ports with 2 mm holes with micropunch (Ted Pella Inc.) for injecting DNA, and two 0.5 mm ports for rinsing. To ensure the surface cleanness of PDMS device, we cleaned with ethanol and IPA, and bonded to a clean glass slide using oxygen plasma for 40 s at low power in 0.65 torr with 7.16 W to result in a nanopore device (Figure 6). KCl and DNA solution was injected right after the treatment of oxygen plasma bonding on the surface of nanopore PDMS devices. Once fabricated, the device was robust, allowing hours of measurement.

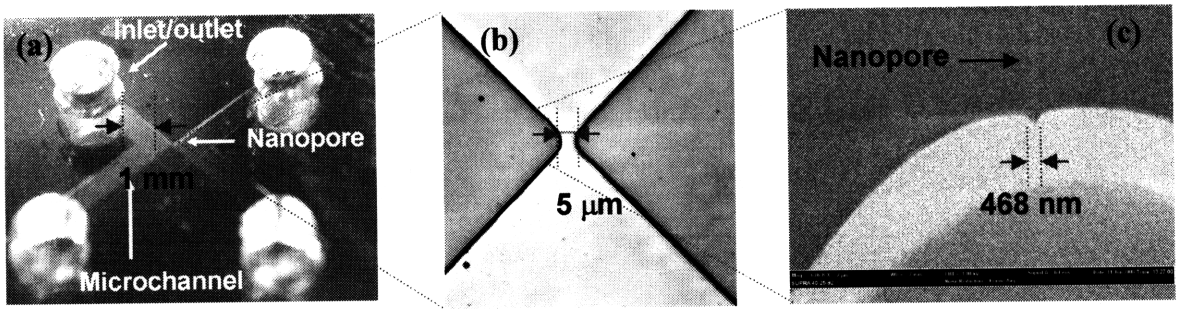

Figure 6 (a) Overview of PDMS nanopore device. (b) Two microchannels connected by a nanopore of 200 × 500 nm × 5 μm. (c) SEM image shows PDMS component before bonding.

2.3 Discussion

During fabrication process, we encountered several issues that initially prevented us from having successful working nanopore sensor device. Below we list the issues by the order of fabrication process.

(1) The cleanness of the silicon wafer is critical to the attachment of SU-8. After we finished the lift-off process for patterning Ti lines on the wafer, it had to be cleaned using air plasma in 7.16 W for at least 40 s. This step could eliminate any organic materials sticking on the wafer in addition to dehydration of the surface. If the wafer was cleaned with ethanol and IPA followed by dehydration, SU-8 would still peel off from the substrate once developed.

(2) Gradually heating the SU-8 microchannel to desired baking temperature was also essential to the attachment of SU-8 to silicon wafer. If the SU-8 was heated directly at desired baking temperature, it would peel off from the substrate once developed.

(3) The curing time and temperature are two critical factors that determine whether PDMS nanopore would collapse. We had previously baked PDMS with 65 °C for 2 hours, and the nanopore collapsed once bonded to the device. Collapse of the nanopore was evident by the lack of scattered light from the collapsed nanopore, making it invisible under the optical microscope (Figure 7).

(4) The cleanness of PDMS and glass surface is essential to ensure proper bonding between PDMS nanopore and glass substrate. After cleaning the PDMS device with ethanol and IPA, the bonding between the PDMS device and glass and also the stability of current signals improved dramatically.

(5) The energy of plasma is also critical to the surface properties of PDMS. When we increased the time of oxidizing from 40 s to 60 s with air plasma at 7.16 W, the surface of PDMS nanopore device became too hard to be bonded to the glass substrate.

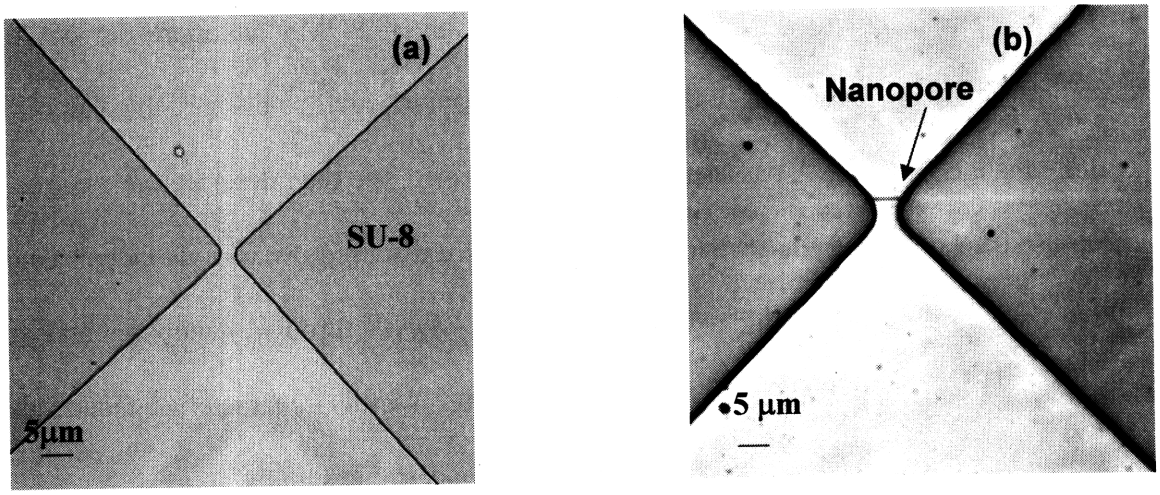

Figure 7 Collapsed v.s. non-collapsed nanopore. (a) Collapsed nanopore. When the nanopore collapsed, the device looked like as if there was no nanopore connecting the two microchannel reservoirs. (b) Non-collapsed nanopore. When the nanopore did not collapse, the nanopore could be seen clearly under optical microscope.

2.4 Conclusion

Here we have successfully fabricated a PDMS nanopore sensor device of 200 × 500 nm × 5 μm. The cleanness of the wafer, the temperature and length of time for baking PDMS, the cleanness of the PDMS surface before bonding to glass slide, and the power of plasma, are all important factors for having a successful nanopore device. In the next chapters we will use these devices for measuring and characterizing the analyte (48.5 kbp λ-DNA) passing through the nanopore.

Chapter 3 Nanopore Device Characterization for Single Molecule Detection

3.1 Introduction:

In the previous chapter, we described the fabrication of PDMS nanopore devices for detecting single molecules of λ-DNA. In this chapter we first discuss the theory of current change when DNA passes through the nanopore. We then describe the electronic setup used for detecting the translocation events. We discuss how various factors could affect the translocation and detection signals of λ-DNA through nanopore, and the possible mechanism of DNA entering the nanopore. We also characterize factors that contribute to the noise of the measurements of these electronic signals.

3.2 Experiment Setup

Here we applied a voltage bias across nanopore, and measured the corresponding ionic current signal. The ionic current was measured using a patch-clamp amplifier (Axopatch 200B, Axon Instruments, Union City, CA). Electrical connections to the device were made with Ag/AgCl electrodes (In Vivo Metric) and current measurements were taken inside a Faraday cage to shield from any electromagnetic interference (Figure 8). The current signal I_{pore} was transferred to the Axopatch amplifier, and filtered by embedded lowpass Bessel filter (80 dB/decade) at 1 kHz cutoff frequency to have maximum signal-to-noise ratio. Filtered current signal was first converted to voltage signal V_I, and then digitized at 20 kHz/16 bits using a Data Acquisition Card (DAQ) (National Instruments PCI-6251M, Austin, TX) installed in a desktop computer. Digitized signal was then

acquired and recorded to computer interfaced with home-built National Instruments LabVIEW program. Magnitude of voltage V_{pore} across nanopore was applied by Axopatch current amplifier, which was controlled by LabVIEW program's output voltage V_v.

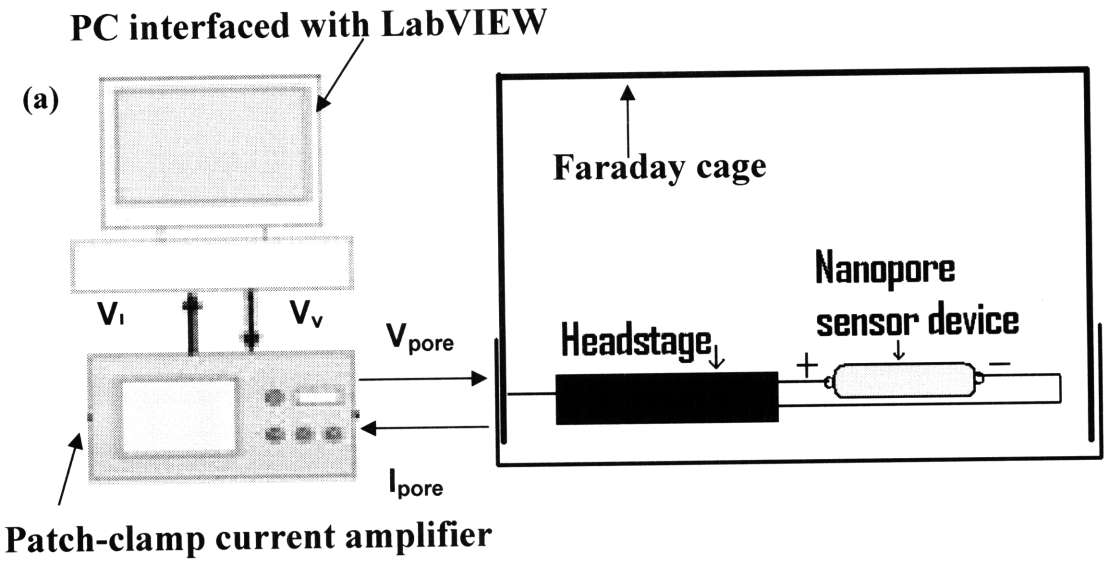

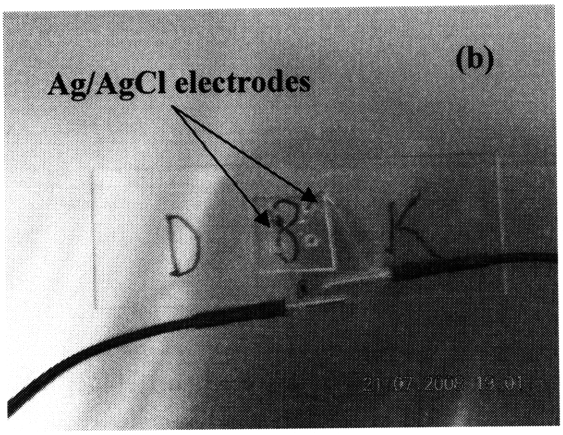

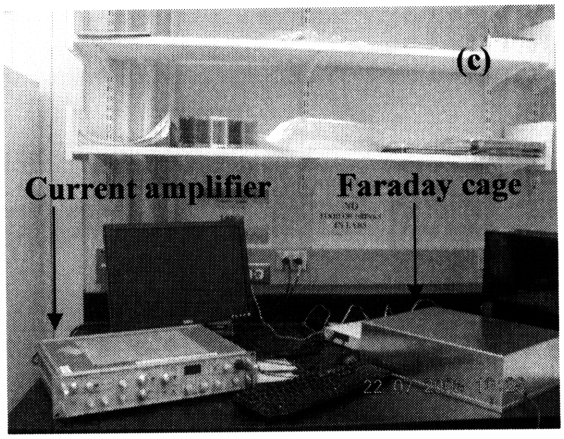

Figure 8 (a) A schematic diagram of the apparatus for measuring the DNA translocation events through PDMS nanopore device. Measurement was done inside a Faraday cage with patch-clamp current amplifier, which was interfaced with PC by LabVIEW software. Current data were continuously saved to disk in the computer. (b) Voltage was applied across nanopore using Ag/AgCl electrodes. D side represents the reservoir with

DNA, while K side represents reservoir with only KCl buffer solution. (c) Photograph of actual experimental setup.

The relation of conversion between measured current value I_{pore} and converted voltage signal V_I was determined by $V_I(mV) = \alpha\beta \times I_{pore}(pA)$, where α is "scaled output gain", and β is "configuration" in Axopatch settings. Higher $\alpha\beta$ gives higher voltage value for a given current value, and therefore has higher resolution. However, the maximum input voltage that can be measured with LabVIEW/DAQ was ± 10 V, which gives an upper limit of output gain. Since the average current measured in the experiment was hundreds of pA, we measured the ionic current in resistive feedback mode so that configuration β was set to "whole cell" mode as recommended by the manufacturer. Combined the limitations and considerations above, we found the optimum value of combination to be $\alpha\beta = 1$ ($\alpha = 1, \beta = 1$ in whole cell configuration). Since the limitation of input voltage for LabVIEW/DAQ is ± 10 V, the maximum current that could be measured was 10 nA.

The ratio (V_{pore}/V_v) between output voltage from Axopatch current amplifier and output voltage from LabVIEW/DAQ is either 100 mV/V or 20 mV/V. Since we desired maximum range of output voltage from Axopatch current amplifier, we used 100 mV/V as the conversion factor. Since the maximum output voltage from LabVIEW/DAQ was ± 10 V, the maximum voltage that could be applied by Axopatch current amplifier was ± 1 V.

For the DAQ card, we chose PCI-6251M because of its high resolution (16 bit) and fast read speed (1 MS/s). In addition, PCI-6251M supports analog output waveform

generation with an analog input trigger. Since our measured signals shared a common ground with the DAQ device, the "differential" measurement mode was used for analog input[56]. The sampling frequency was set to be 20 kHz since it is enough to characterize the translocation signals of DNA molecules. Since we manually controlled output voltage value, the generation mode was "1 sample (on demand)". In addition, we used real-time Fast-Fourier-Transform (FFT) to obtain the power spectrum of the measured signal, thus having access to inspect the source of the noise in real time.

3.3 Theory for Current Change due to Translocation of λ-DNA through Nanopore

Here the calculation of current change is based on the molecules of 48.5 kbp λ-DNA in KCl buffer solution, and the size of the nanopore is 200 nm × 500 nm × 5 μm. The transport of λ-DNA can affect the current in two ways[14, 34]: (i) change of ionic concentration, and (ii) blockage of nanopore with λ-DNA. While mechanism (i) tends to dominate at low buffer concentration, mechanism (ii) tends to dominate at high buffer concentration. The two competing effects cancel at a KCl concentration of ~0.37 M[22].

For mechanism (i) that dominates in low buffer concentration, the current increases due to the negative charges on DNA molecules. The translocation of DNA will induce additional counterions (K^+ ions) to neutralize the net charges of DNA within the pore, and therefore the ionic current will increase[14, 33, 34]. The expected current increase is given by:

$$\Delta I_1 = \mu b \Delta n e \frac{V}{L_{pore}^2} \quad \text{.....(1)}$$

Where Δn is the number of charges introduced uniformly into a nanopore of length L_{pore} with a voltage bias V applied across it, e is charge of an electron, μ is ionic mobility, and b is the fraction of mobile counterions[14]. With an ionic mobility of 7.9×10^{-8} m^2/Vs for KCl, $b = 0.5$, $\Delta n = 97004$, $L_{pore} = 5$ μm, and $V = 0.5$ volt, we expected the magnitude of current increase $\Delta I_1 \approx 12$ pA.

For mechanism (ii), bulk ionic current would decrease due to physical blockage by the DNA molecules. For particles of diameter much smaller than that of the nanopore, previous work on colloids[4] has shown that the ratio of peak height ΔI_1 to open pore ionic current I is approximately equal to the volume ratio of particle $V_{particle}$ to pore V_{pore}:

$$\frac{\Delta I_1}{I} = \frac{V_{particle}}{V_{pore}} \quad \text{..... (2)}$$

Where the theoretical open nanopore ionic current I under voltage bias V is:

$$I = \frac{V \sigma A}{L_{pore}} \quad \text{..... (3)}$$

The radius of DNA strand $R = 1.1$ nm and the corresponding DNA length $L_{DNA} = 48502 \times 0.34$ nm $= 16.5$ μm, the volume $V_{particle}$ of λ-DNA would be $\pi \times R^2 \times L_{DNA} = 62341.8$ nm^3. As we have pointed out in section 3.2, the maximum ionic current that could be measured in our system is ± 10 nA. Therefore, from equation (1) maximum current change that can be measured due to blockage with single molecules of DNA in 200 nm × 500 nm × 5 μm nanopore is 10 nA × $(\frac{V_{particle}}{V_{pore}}) \approx$ 1.2 pA, which is much smaller than the current change due to mechanism (i).

We therefore come to the conclusion that it is desirable in our system to use *low* buffer concentration so that the mechanism of current change when λ-DNA passes through the nanopore would be dominated by current *increase*.

Moreover, we now calculate the net current change $\Delta I = \Delta I_1 - \Delta I_2$ for DNA translocation events in 10 mM KCl solution. Here σ = conductivity of 10 mM KCl = 0.1332 Ω^{-1} m^{-1}, A = cross section area of the nanopore = 200 nm × 500 nm, L_{pore} = 5 μm, and V = 0.5 V. The theoretical open nanopore ionic current I is 1.33 nA. From equation (2), the magnitude of current decrease due to mechanism (ii) is $\Delta I_2 = I \times (\frac{V_{particle}}{V_{pore}}) \approx 0.13$ pA.

Since current increase ΔI_1 due to mechanism (i) was calculated to be about 12 pA, the net current change is $\Delta I = \Delta I_1 - \Delta I_2 \approx 12$ pA.

3.4 Detection of λ-DNA

In section 3.3 we discussed why it is desirable to measure the translocation events of λ-DNA in *low* buffer concentration. We used 48.5 kbp long λ-DNA since it could be detected more easily than other shorter DNA strands with less negative charges. A voltage bias of -0.5 V was applied across 200 nm × 500 nm × 5 μm nanopore with 10 μg/mL λ-DNA on only one side of the nanopore in 10 mM KCl buffer solution. The baseline current was about 1.35 nA, and the peak height due to DNA translocation was ~14 pA with a duration of 50 ms (Figure 9 (a)), which was in the expected range based on equations (1) to (3). A control experiment was done by reversing the bias polarity, and no translocation signals were observed, thus confirming that these events were due to translocation of λ-DNA (Figure 9(b)).

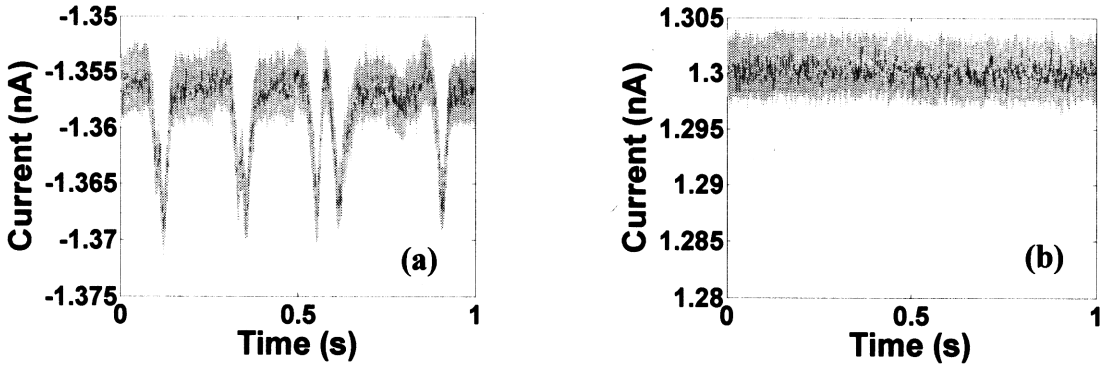

Figure 9 (a) Translocation signal obtained for a 10 μg/mL λ-DNA sample with a voltage bias of -0.5 V. Current increases by about 14 pA during the translocation due to charge effect. (b) No translocation signals were observed when bias polarity was reversed.

Moreover, we observed that baseline current kept increasing during the measurement, which suggested that DNA might get stuck inside the nanopore. One possible solution is to coat the nanopore device with serum albumin (BSA) that could significant improve the device's stability by preventing aggregation of DNA molecules in the nanopore. Figure 10 (a) shows that without coating PDMS nanopore with BSA, nanopore got stuck easily compared to that coated with 1mg/mL BSA in figure 10 (b). Moreover, the peak height of DNA translocation signals did not change significantly, verifying that these events were still due to translocation of DNA molecules. In addition, sticking problem also occurred when using solution of 1 % solid content of 100 nm plain polystyrene nanoparticles functionalized with carboxyl function groups (Phosphorex Inc., MA). Figure 11 (a) and figure 11 (b) show the huge differences between each peak heights, which could be multiple nanoparticles sticking into the nanopore, or the deformation of the nanopore due to the translocation of particles.

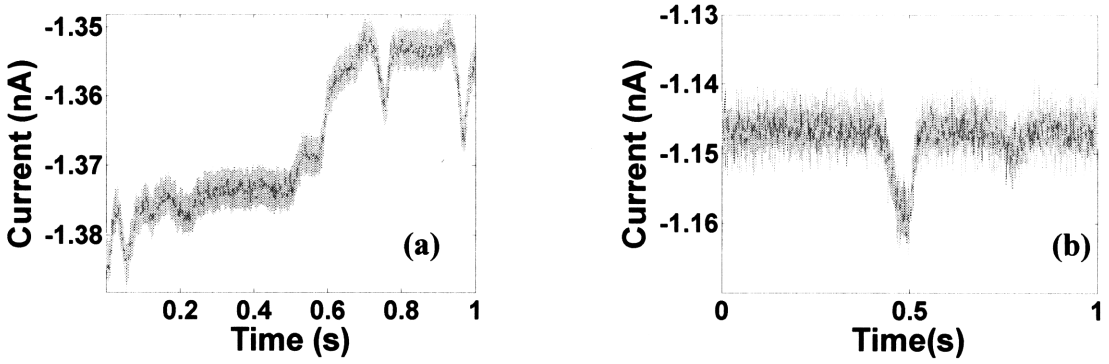

Figure 10 (a) PDMS nanopore without BSA. Nanopore device becomes unstable due to sticking with DNA molecules. (b) PDMS nanopore coated with 1mg/mL BSA.

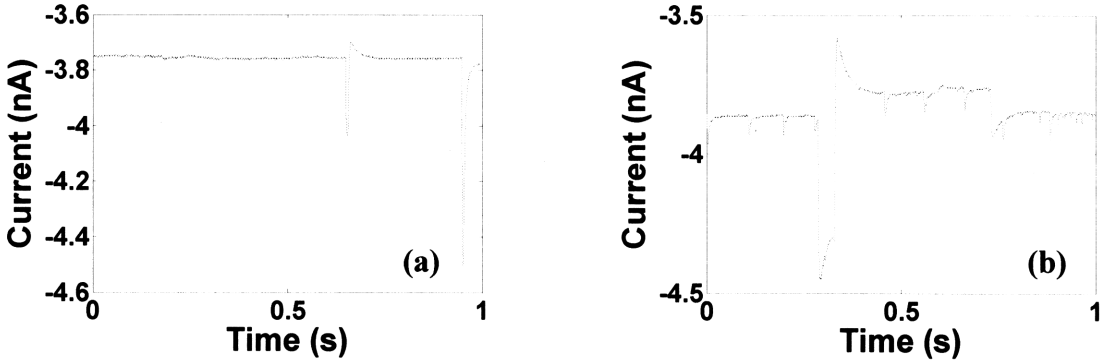

Figure 11 Translocation signals of 100 nm nanoparticles through PDMS nanopore without BSA. (a) No sticking. Open nanopore current did not change (b) Sticking results in unstable open nanopore current.

3.5 Characterization of DNA Inter-translocation Time and Factors Affecting DNA Translocation

The frequency of DNA translocation events and signal-to-noise ratio are critical factors toward successful implementation of multiple measurements on the same molecule. When the rate of translocations is high, it is more likely that the trapped molecule which is supposed to be recaptured by the nanopore would be displaced by another molecule

entering the pore. In addition, the signal-to-noise ratio is essential to the successful detection and following feedback control for multiple measurements. Intuitively, factors such as magnitude of voltage applied across nanopore, analyte concentration, and dimension of the nanopore would affect the rate of DNA translocation events and signal-to-noise ratio. In 3.5.1 we characterize the relation between magnitude of voltage and inter-translocation time, and in 3.5.2 we characterize factors that affect signal-to-noise ratio and rate of DNA translocation events.

3.5.1 Characterization of DNA inter-translocation

Here inter-translocation time T is defined as the time interval between the *starts* of two consecutive DNA translocation events. We characterize the translocation events by inspecting the relation between DNA inter-translocation time T and applied voltage bias. Translocation events took place when a voltage bias of 0.5 V or higher was applied across 200 nm × 500 nm × 5 μm nanopore with 5 μg/mL λ-DNA on only one side of the nanopore in 10 mM KCl buffer solution. Figures 12 (a) to figure 12 (f) show histograms of DNA inter-translocation time with 6 different magnitudes of applied voltage in a period of 79 s of measurement. It is seen that overall the number of DNA translocation events increased with magnitude of voltage. Also, larger voltage bias leads to higher percentage of shorter inter-translocation time events.

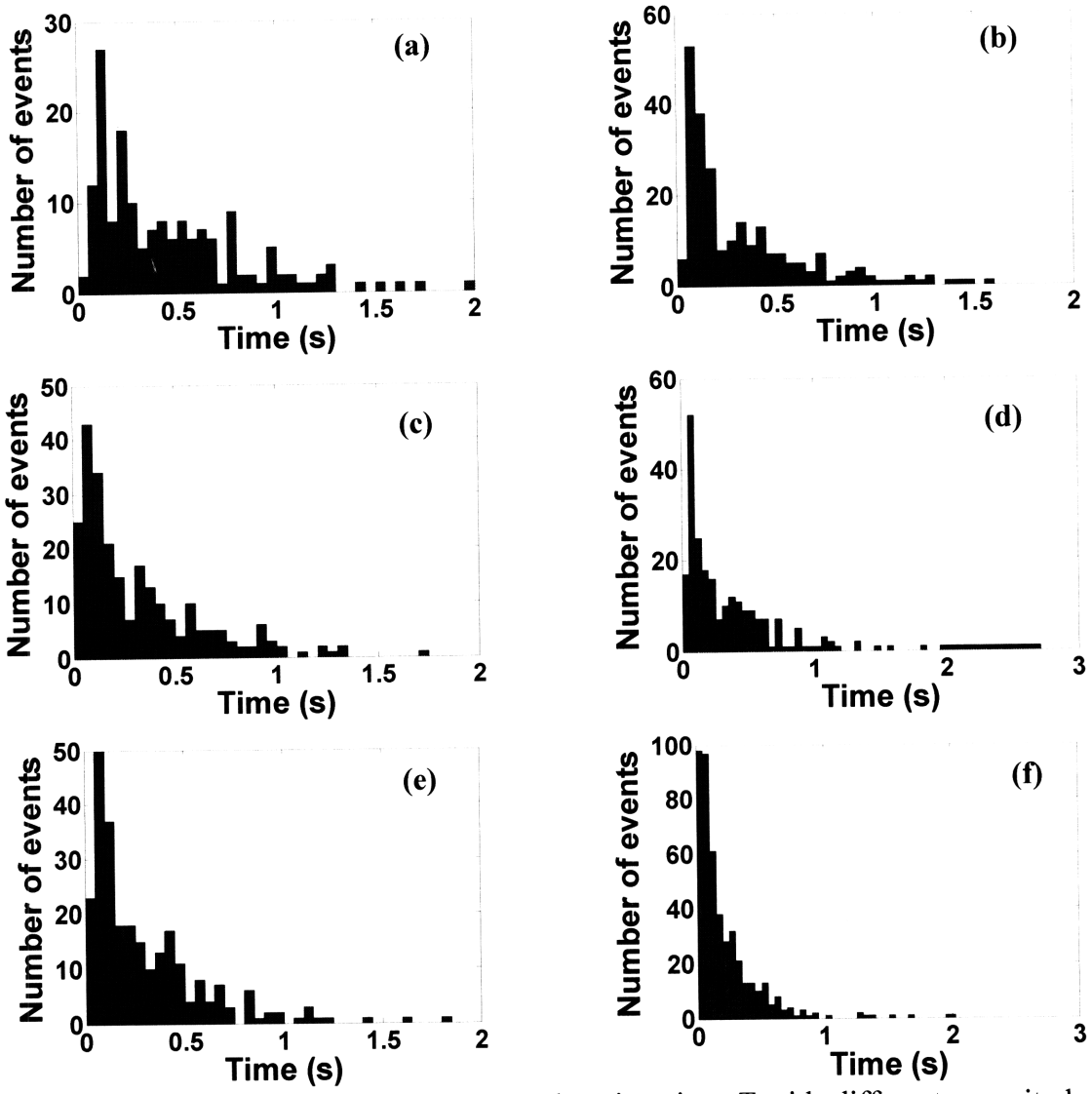

Figure 12 Histograms of DNA inter-translocation time T with different magnitudes of voltage in 79 s of measurement. (a) 0.5 V (b) 0.6 V (c) 0.7 V (d) 0.8 V (e) 0.9 V (f) 1 V Each column represents a time interval of 50 ms.

We tried to verify whether DNA translocation event through the nanopore *after* previous DNA translocation has been completed is a Poisson process[43]. Here the inter-arrival time t is defined as time interval between the *completion* of last DNA translocation and the *start* of subsequent DNA molecule translocation event through nanopore, and is t is

assumed to be equal to the length of inter-translocation time T minus average DNA translocation time t_0. In other words, we tried to verify whether the events distribution graph of DNA inter-arrival time t would be the same as the inter-arrival time in a Poisson process. The probability density function of inter-arrival time in the Poisson process is $f(t) = \lambda e^{-\lambda t}$, where $\lambda =$ average value of inter-arrival time. Since $T = t + t_0$, the probability that inter-translocation time T ($T \geq t_0$) falls between $t_0 + t_1$ and $t_0 + t_2$ is:

$$P(t_1+t_0 \leq T \leq t_2+t_0) = e^{-\lambda t}\Big|_{t=t_1} - e^{-\lambda t}\Big|_{t=t_2} \quad \text{.....(4)}$$

Moreover, since the average DNA translocation time t_0 decreases with the increase of voltage, the minimum inter-translocation time ($T_{min} = t_0$) for which we extracted the events increases with the decrease of voltage. We found that DNA average translocation time t_0 = 120 ms for 0.5 V, 110 ms for 0.6 V, 95 ms for 0.7 V, 85 ms for 0.8 V, 70 ms for 0.9V, and 65 ms for 1 V. Figure 13 (a) to figure 13 (f) show the corresponding histogram and the theoretical (red) curve of Poisson process calculated as above. Each column represents a time interval of 50 ms. It is shown that the theoretical Poisson curve is close to corresponding histogram, especially for intervals of higher inter-arrival time.

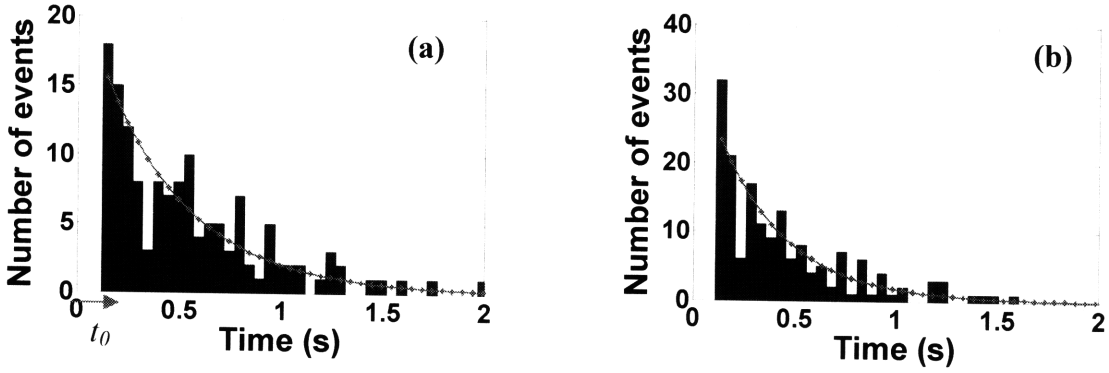

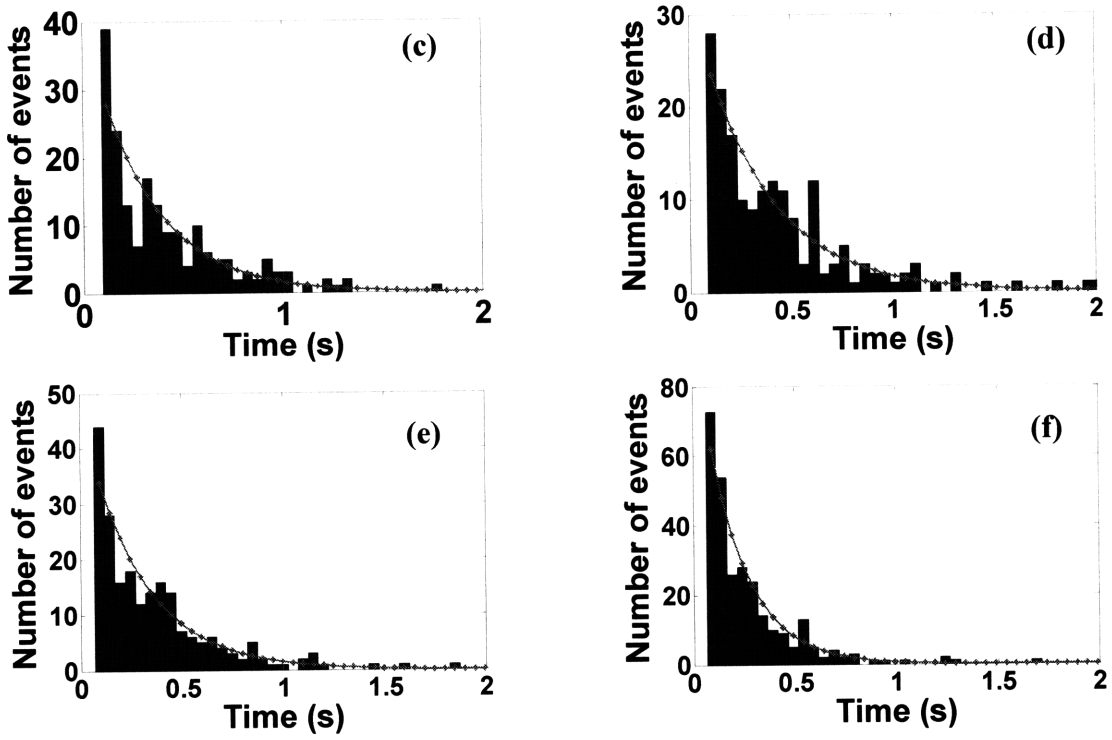

Figure 13 Poisson approximation for histograms of DNA's inter-translocation time T that is larger than DNA average translocation time t_0. Each graph represents events at different magnitude of applied voltage. (a) 0.5 V (b) 0.6 V (c) 0.7 V (d) 0.8 V (e) 0.9 V (f) 1 V. Each bar represents a time interval of 50 ms starting at $t = t_0$ to $t = t_0 + 50$ ms.

3.5.2 Factors affecting DNA translocation

For a polymer to be hydrodynamically driven into nanopore that is smaller than the radius of gyration of the polymer, Daoudi et al.[53] showed that there is a critical polymer concentration c*, the polymer overlap concentration, below which the critical hydrodynamic flux is independent of the polymer concentration c, polymer size, and pore sizes.

In Daoudi et al.'s paper, the hydrodynamic force is linearly proportional to the velocity of the strand, and therefore linear with the relative local hydrodynamic velocity of the

strands. In our system where DNA is driven by electric field, the electric force on our DNA molecules is linearly proportional to the electric field on the molecule, and therefore linear with the ionic current density around the entry of the nanopore. In addition, the size of our PDMS nanopore (200 nm×500 nm) is smaller than the radius of gyration R_g of 48.5 kbp DNA (0.7 μm)[57]. We therefore expect that there will be a similarity between hydrodynamically driven mechanism in Daoudi et al.'s paper and our electrically driven system. Specifically, if DNA concentration in our system falls below overlap concentration c^*, the critical ionic current above which λ-DNA could be electrically driven into the nanopore is independent of DNA concentration and nanopore size.

Here we calculate the overlap concentration c^* in our system by assuming the positions of DNA molecules in KCl solution would be in simple cubic arrangement. The critical number of DNA molecules that would start to overlap with each other in 1 mL solution is $\frac{1\,\text{mL}}{(2R_g)^3}$. Since the molecular weight of 48.5 kbp dsDNA is 48500×660 g/mol, the overlap concentration c^* of DNA is $\frac{1\,\text{mL}}{(2R_g)^3} \times \frac{48500 \times 660}{6 \times 10^{23}} = 19.5$ μg/mL.

Sohn et al.[16] detected DNA translocation signal in 200 nm × 200 nm × 3 μm PDMS nanopore. However, they did not detect translocation signal when the height of the nanopore was above 300 nm. Since the increase of the nanopore's height increases the ionic current density for a given voltage, the translocation events should increase according to theory of polymer translocation theory stated above. Therefore, it could be suggested that the translocation signals are too small to be detected in their system.

Han et al.[57] showed that there are two major time scales, transport time and entrance time, that determine the length of time it takes when driving DNA electrically from a large microchannel into a 90 nm slit. Transport time is defined as the time it takes for DNA to transport from microchannel to the entrance of the slit. Entrance time is defined as the time it takes for DNA to enter the nanopore. When transport time dominates, the frequency of translocation events depends on the concentration of DNA. When the entrance time dominates, the frequency of translocation events is independent of the concentration of DNA.

Here we tried to characterize factors that would affect signals of DNA translocation events in our system. Figure 14 (a) and (b) showed when decreasing the magnitude of voltage from -0.5 V to -0.4 V with the same DNA concentration (5 μg/mL) in 200 nm × 500 nm × 5 μm nanopore, the number of DNA translocation events significantly changed. This illustrates that the critical voltage required to drive DNA into the nanopore is about 0.4 V, and the corresponding current is about -0.92 nA in 10 mM KCl. Figure 15 (a) and (b) showed that increasing the nanopore length from 5 μm to 8 μm with the same voltage bias (-1V) and DNA concentration (5 μg/mL) yields poor signal-to-noise ratios.

In addition, we compared DNA translocation rate with different DNA concentration at different voltages in the same device. Here we measured the relation between DNA translocation rate and voltage with concentration of 0.625 μg/mL, 1.25 μg/mL, and 7.5 μg/mL in 200 nm × 500 nm × 8 μm nanopore device. The results in figures 16 (a) and (b) showed that translocation rate increased with the increase of concentration and voltage bias. As the concentration of DNA increased, the voltage at which we started to

have DNA translocation event decreases slightly. Since the DNA concentrations we used were all well below overlap concentration c^* of 19.5 μg/mL calculated before, we observed that critical ionic current and therefore the critical voltage at which translocation events occurred did not change significantly with DNA concentration, and time scale was dominated by transport time, which results in a linear relationship between concentration and rate of translocation events.

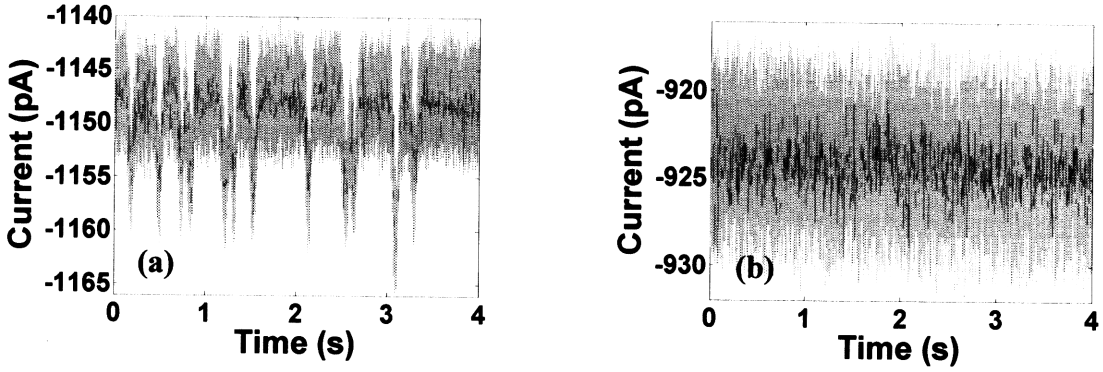

Figure 14 Comparison of number of translocation events at different voltage. (a) Voltage bias of -0.5V in 200 nm × 500 nm × 5 μm nanopore. (b) Voltage bias of -0.4V in 200 nm × 500 nm × 5 μm nanopore. Voltage bias smaller than 0.5 V results in no translocation signals in length of 5 μm nanopore with 5 μg/mL λ-DNA.

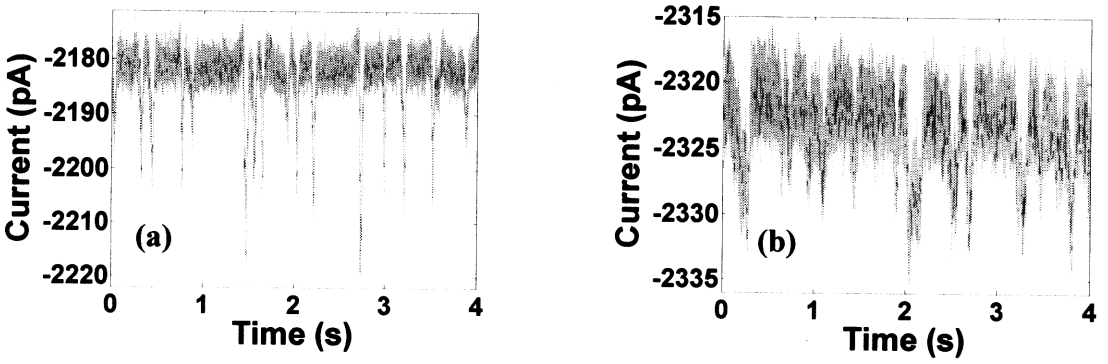

Figure 15 Comparison of signal to noise ratio with different lengths of nanopore. (a) Voltage bias of -1 V in 200 nm × 500 nm × 5 μm nanopore. (b) Voltage bias of -1 V in 200 nm × 500 nm × 8 μm nanopore. Signal-to-noise ratio significantly decreases with longer length.

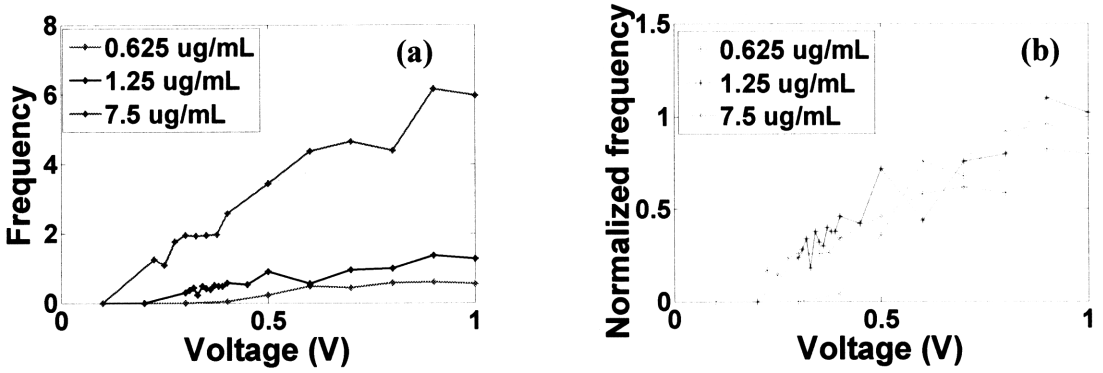

Figure 16 (a) Frequency of DNA translocation events with different voltage bias and DNA concentrations. Blue line represents DNA concentration of 7.5 μg/mL, black line represents DNA concentration of 1.25 μg/mL, and red line represents DNA concentration of 0.625 μg/mL. (b) Events frequency normalized with DNA concentration.

3.6 Characterization of Noise in the System

The main objective of this work is to enhance measurement capability of PDMS nanopore. We therefore tried to characterize several factors that contribute to the noise of the measurement. This characterization could be used a basis to determine optimal operating conditions such as the length of the nanopore and buffer concentration.

Here we characterized how Axopatch patch-clamp current amplifier, concentration of buffer solution, addition of BSA, and type of the device affect the magnitude and

spectrum of the noise. All the measurements were done without applying voltage bias for period of 5 s with sampling rate of 20 kHz. The dimension of the nanopore used in this experiment was 200 nm × 500 nm × 8 μm. Figures 17 (a) to (n) show measured current signals with different conditions and corresponding noise power spectrum. To summarize the effects of noise from each factor, we determined the noise's root-mean-square (RMS) value for each experimental condition with three different time intervals of windowing (Figure 18).

When measuring electronic signals with Axopatch current amplifier being turned off, the RMS noise is about 0.71 pA, which is the noise contribution coming from LabVIEW/DAQ connection board. When measuring across nanopore in 10 mM KCl with BSA coated on the device, the RMS noise is about 0.28 pA larger than that without BSA. This suggests that BSA contributed to the RMS noise for about 0.28 pA. When measuring across nanopore in 100 mM KCl , RMS noise is about 0.22 pA larger than that in 10 mM KCl. When measuring across microchannel in 100 mM KCl with BSA coated on the device, the RMS noise is about 4.15 pA larger than that in 10 mM KCl. This suggested that the RMS noise increases more rapidly when the equivalent resistance between the electrodes is lower. From the analysis of noise power spectrum, the increase of the noise comes mainly from flicker (1/f) noise and white noise. Moreover, when measuring across microchannel in 100 mM KCl with BSA, the RMS increased dramatically with the increase of time interval windowing from 1 s to 3 s. This indicated that the low frequency noise (< 1 Hz) dominated the noise power spectrum under this experiment condition.

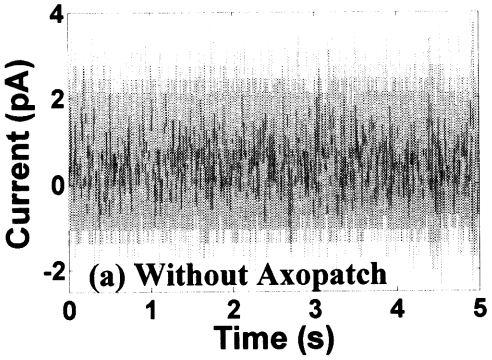
Current (pA)
Time (s)
(a) Without Axopatch

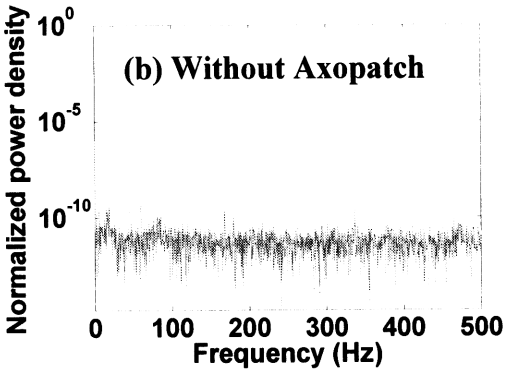
Normalized power density
Frequency (Hz)
(b) Without Axopatch

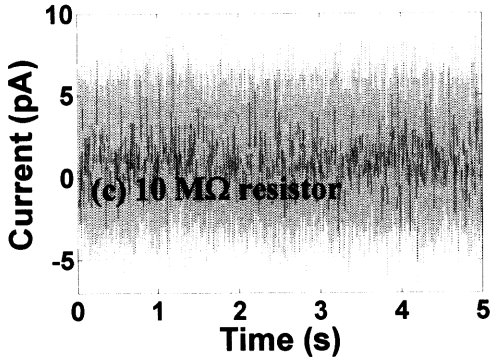
Current (pA)
Time (s)
(c) 10 MΩ resistor

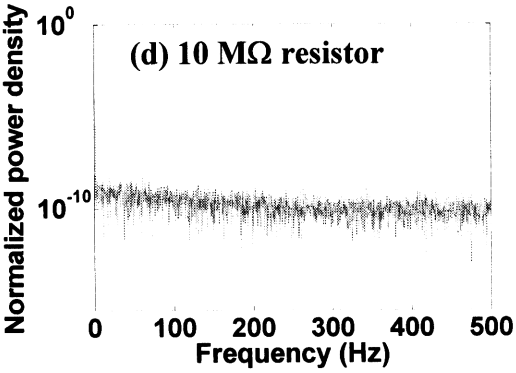
Normalized power density
Frequency (Hz)
(d) 10 MΩ resistor

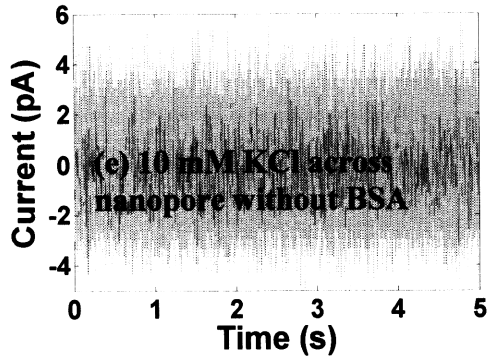
Current (pA)
Time (s)
(e) 10 mM KCl across nanopore without BSA

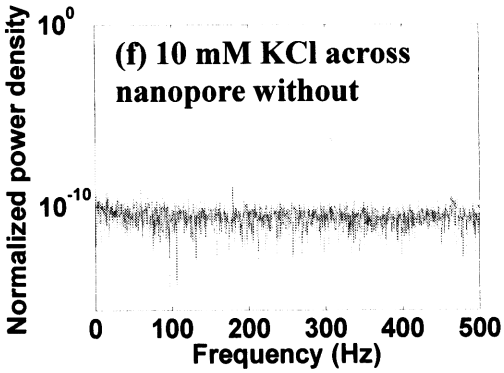
Normalized power density
Frequency (Hz)
(f) 10 mM KCl across nanopore without

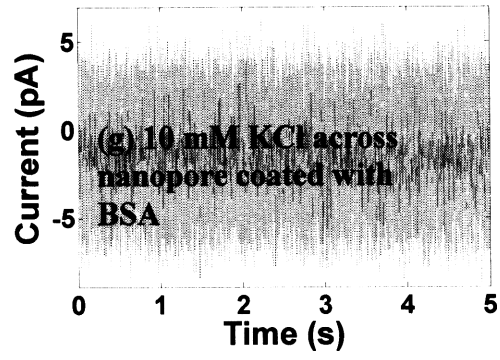
Current (pA)
Time (s)
(g) 10 mM KCl across nanopore coated with BSA

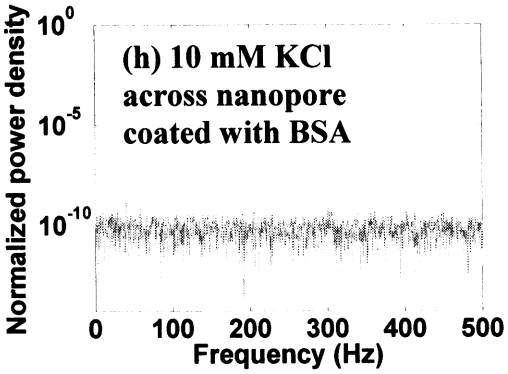
Normalized power density
Frequency (Hz)
(h) 10 mM KCl across nanopore coated with BSA

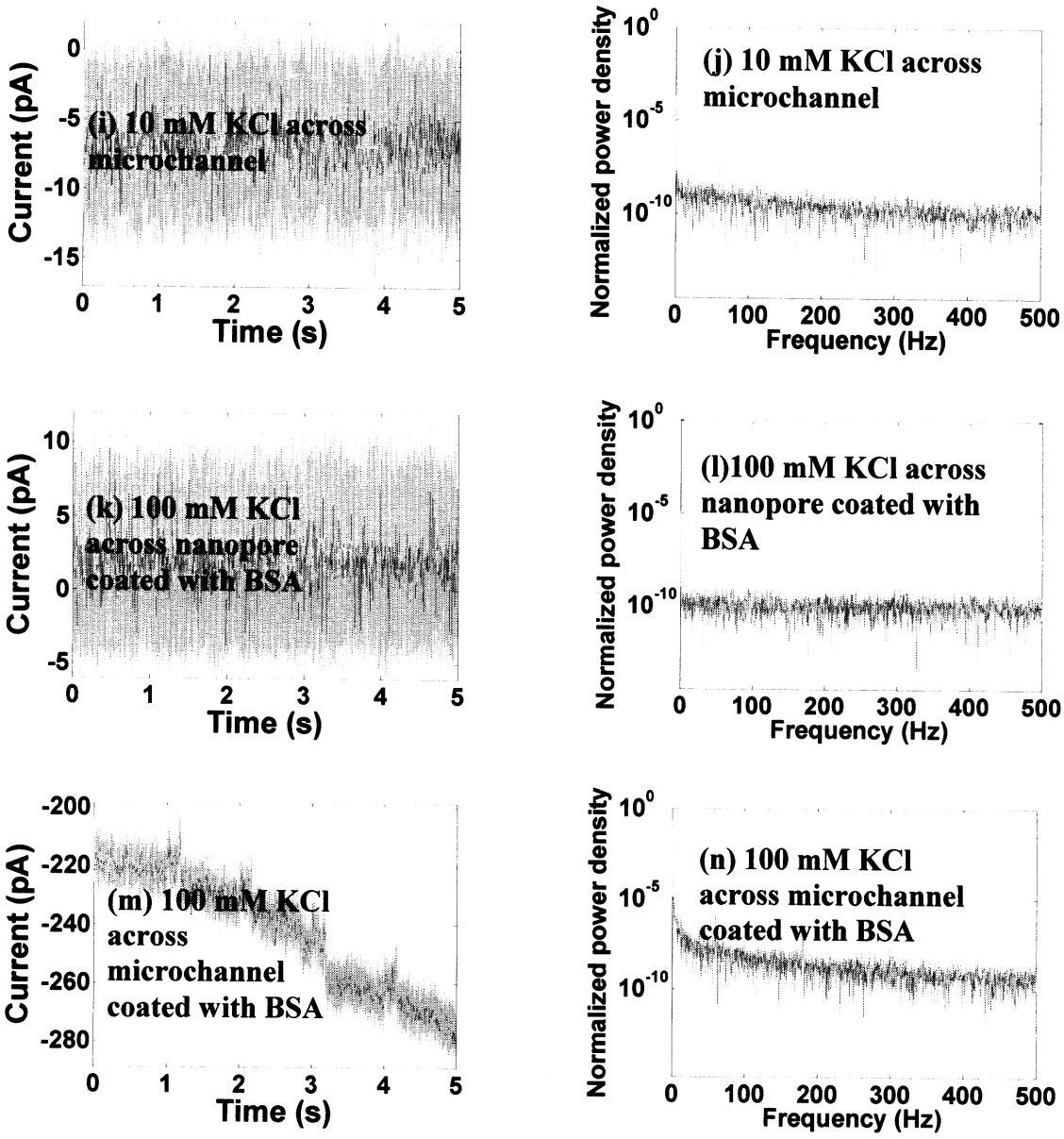

Figure 17 Ionic current and corresponding Fast Fourier Transform with different factors. Voltage bias is 0 V, and dimension of nanopore device is 200 × nm × 500 nm × 8 μm. (a) and (b) Measurement without Axopatch patch-clamp current amplifier. (c) and (d) Measurement across 10 MΩ resistor. (e) and (f) Measurement of 10 mM KCl across nanopore without BSA coated. (g) and (h) Measurement of 10 mM KCl across nanopore coated with BSA. (i) and (j) Measurement of 10 mM KCl across microchannel. (k) and

(l) Measurement of 100 mM KCl across nanopore coated with BSA. (m) and (n) Measurement of 100 mM KCl across microchannel coated with BSA.

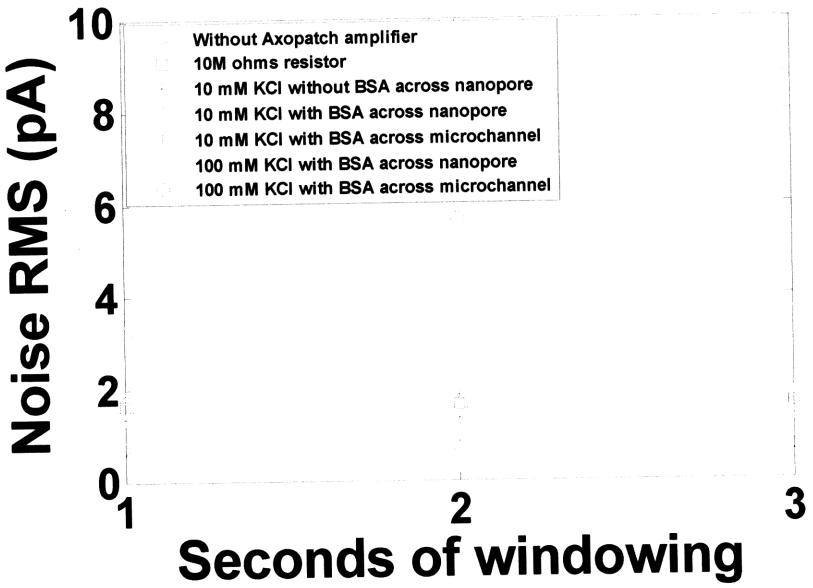

Figure 18 Root-mean-square (RMS) value of noise for each experiment condition.

3.7 Conclusion

In this chapter we showed successful detection of λ-DNA with our PDMS nanopore devices. By inspecting DNA inter-arrival time, we showed that DNA translocation events through the nanopore *after* previous DNA translocation has been completed are similar to a Poisson process. Several factors such as the addition of BSA, length of nanopore, magnitude of voltage, and DNA concentration affect number of DNA translocation events and signal-to-noise ratio. We observed that a critical voltage was required to drive DNA into the nanopore. In addition, the linearity of translocation rate with DNA concentration indicated that the translocation rate was limited by transport of DNA to the nanopore. Finally, we characterized the source of the noise under different

experiment conditions, and found out the major increase of the noise come from 1/f flicker noise and white noise.

Chapter 4 Multiple Measurements on the Same Molecule with Feedback Control

4.1 Introduction

In most of the existing designs of nanopores, the analyte molecule escapes into the solution after a single measurement. Nanopore sensing techniques measuring only one translocation of a given molecule may be insufficient to distinguish differences between different molecules in a given sample. In this chapter we implemented multiple (two) measurements on the same particle to increase the signal-to-noise ratio. Upon detection of a translocation event, the applied voltage was reversed, causing the same molecule to traverse back-and-forth through the nanopore. Feedback control was used to reverse the applied voltage bias and thus ensure multiple translocations of a molecule through the nanopore. Signal-to-noise ratio would be expected to increase due to statistically averaging over the measurement[58].

Other approaches for implementing multiple measurements include use of optical tweezers to control transport of DNA[37] or biochemical supramolecular assembly to lock a DNA molecule across a nanopore[59]. The approach used in the thesis is much simpler and more widely applicable for sizing a variety of particles and molecules as it uses feedback control to reverse the applied voltage and thereby reverse the direction of transport of molecules through the nanopore. During the progress of this thesis, Golovchenko et al. implemented feedback control with voltage reversal which enabled multiple measurements on the same molecule of DNA as many as 22 times[44]. However, the recapture probability in their system is low (70%) due to the configuration that consists of a nanopore in a membrane.

With the fabrication process of soft-lithography used in the thesis, it would be feasible to implement a nanopore sensor device consisting of a nanopore and two nanochannel reservoirs on either side. The nanofluidic reservoirs will function as a trap to localize the molecule in the system after translocation through the nanopore, therefore significantly increasing the recapture rate (Figure 19). In this chapter, we explain in detail the implementation of the feedback for multiple measurements, the experiment results, and future directions.

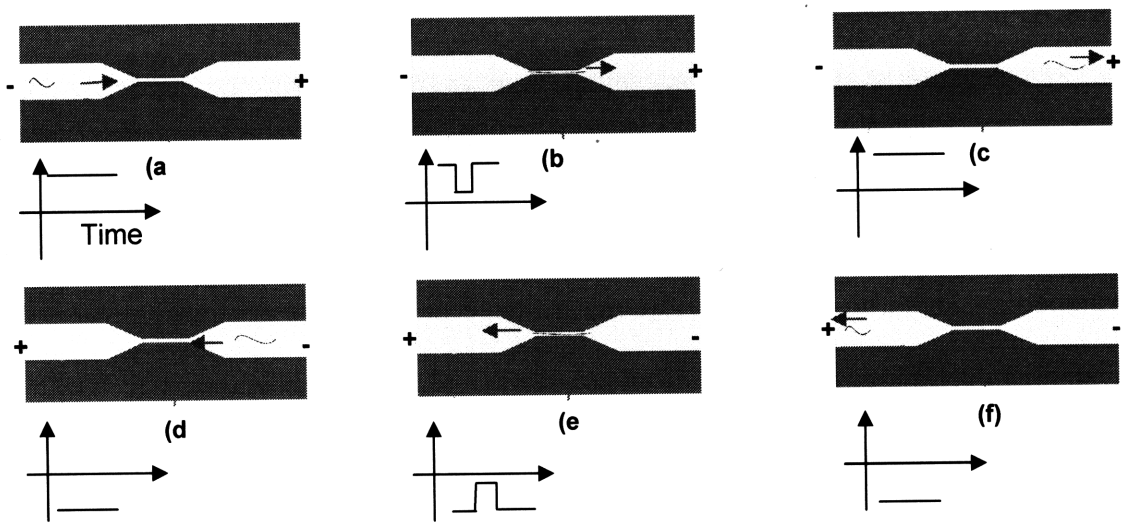

Figure 19 Manipulation of DNA in a PDMS nanochannel-nanopore system for multiple measurements on a single molecule. (a) DNA in the left reservoir, ionic current value equals to open-channel value. (b) When DNA translocates through the pore, the ionic current goes down. (c) DNA in right reservoir, ionic current goes back to open-channel value (d) DNA is electrically driven from right reservoir, ionic current value equals to open-channel value (e) When DNA traverses through the pore, the ionic current decreases. (f) DNA in left reservoir, ionic current goes back to open-channel value.

4.2 Experimental Setup

The electronic hardware setup is the same as that used in Chapter 3 for measuring the single translocation events of λ-DNA. LabVIEW software is also used here for implementing feedback control.

The concept of the algorithm (Figure 20) is to (1) first detect the *entry* of a single DNA molecule into the nanopore, which results in an increase in the ionic current. Then, (2) detect the *escape* of this DNA molecule out of the nanopore, which subsequently decreases the ionic current. (3) Upon detection of the escape of the molecule, reverse the voltage bias to translocate this DNA molecule back into the nanopore for the next measurement.

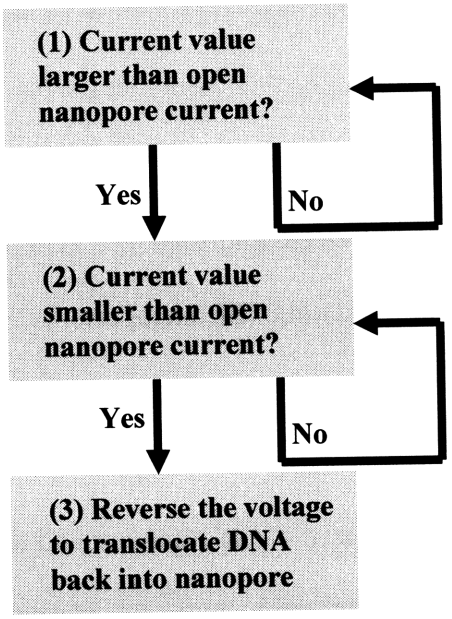

Figure 20 Flow chart of feedback control for multiple (two) measurements.

Below we describe this algorithm in detail (Figure 21).

(A) We measured the ionic current value in real time t_o, and compared it with the open nanopore current (ionic current value without DNA passing through the nanopore). Since there is a continuous drift for open nanopore current, its value was obtained by averaging ionic current from (t_o -12) ms to (t_o -9) ms (yellow arrow). We compared this current value with real time ionic current value, which was obtained by averaging ionic current from (t_o -3) ms to t_o ms (black arrow).

(B) When real time current is larger than the open nanopore current by a specified amount (8 pA in this case), we start comparing the real-time ionic current with open nanopore current obtained until the real-time ionic current *returns* to the value open nanopore current in (A) step. As mentioned before, the increase of real-time ionic current is due to the *entry* of DNA into the nanopore. Since the magnitude of peak of current increase is about 13 pA, we set the criterion of 8 pA to ensure the *entry* of DNA event could be detected.

(C) When the real time current value returns to the open nanopore current obtained in (A), we count this event as one DNA translocation. The decrease of real-time current indicates that DNA has tranlocated out of the nanopore.

(D) Upon detection of the escape of the molecule, voltage bias is reversed in order to translocate this DNA molecule back into the nanopore for second measurement. However, due to the processing speed of the computer and the LabVIEW code used at the time, there was a time delay of ~60 ms between the escape of molecule and the reversal of voltage bias.

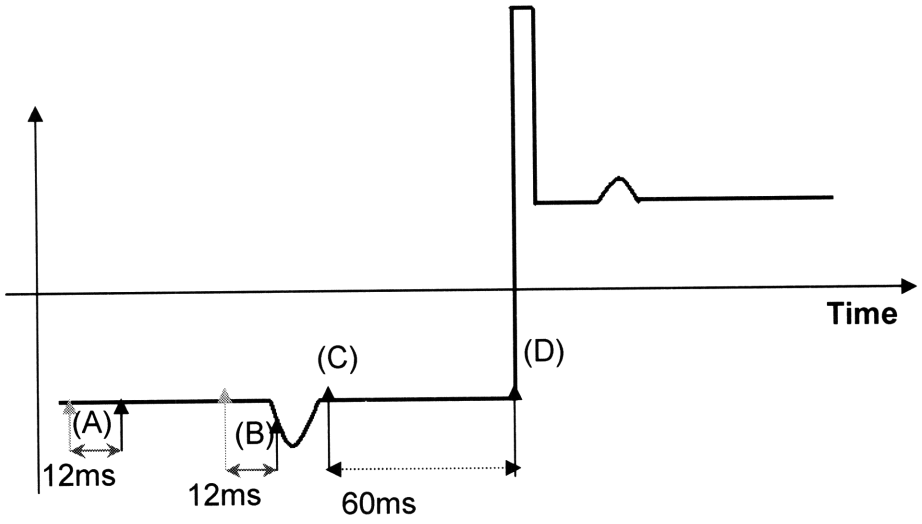

Figure 21 Schematic illustration of feedback control. Orange arrow corresponds to open pore nanopore current, black arrow represents real-time ionic current. (A) Compare real-time ionic current value with open nanopore current to see whether it is larger than open nanopore current. (B) Compare ionic real time current value with open nanopore current to see whether it returns back to open nanopore current. (C) When the real time current value returns to the open nanopore current obtained in (A), we count this event as one DNA translocation. (D) A delay of ~60 ms between the escape of molecule and the reversal of voltage bias.

During the progress of this experiment, the current transient ("overshoot") behavior (Figure 22 (a)) right after voltage reversal in low KCl concentration was the problem that mistakenly triggers voltage reversal before DNA translocates back into the pore. We therefore first implemented two measurements for a given DNA molecule translocation event as proof-of-concept experiment. In addition, the transient effect is larger in 10 mM KCl compared to 1 M KCl (Figure 22 (b)), suggesting that concentration polarization may contribute to the current transients.

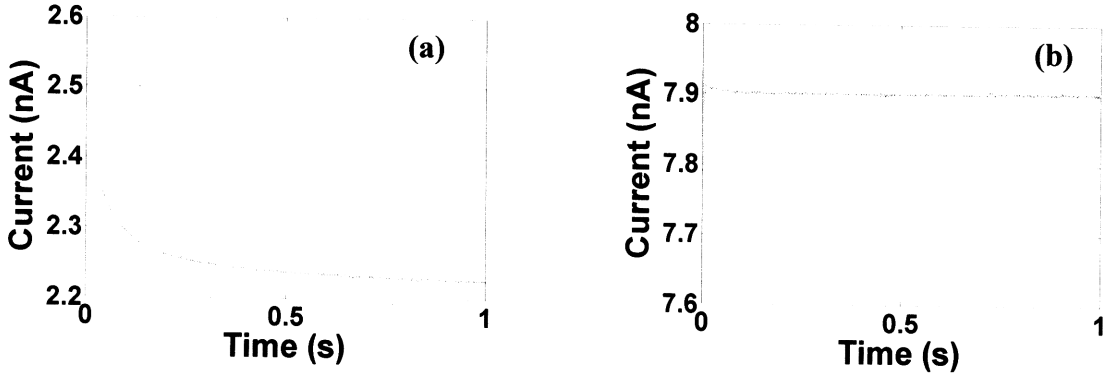

Figure 22 (a) Current value with 10 mM KCl buffer solution immediately after voltage reversal. Transient "overshoot" high current is observed due to concentration polarization.

(b) Current value with 1 M KCl buffer solution immediately after voltage reversal.

4.3 Experiment Results

In the experiment, we applied a voltage bias of ± 1 V across 200 nm × 500 nm × 5 μm nanopore with 7.5 μg/mL λ-DNA in 10 mM KCl on only one side of the nanopore. A translocation signal was observed immediately upon voltage reversal, indicating that the molecule reversed its direction and passed through the nanopore for the second time (Figure 23 and figure 24). Control studies using only buffer or immediate voltage reversal before any translocation was detected did no show any translocation signal, thus confirming that these events were due to λ-DNA going back through nanopore (Figure 25).

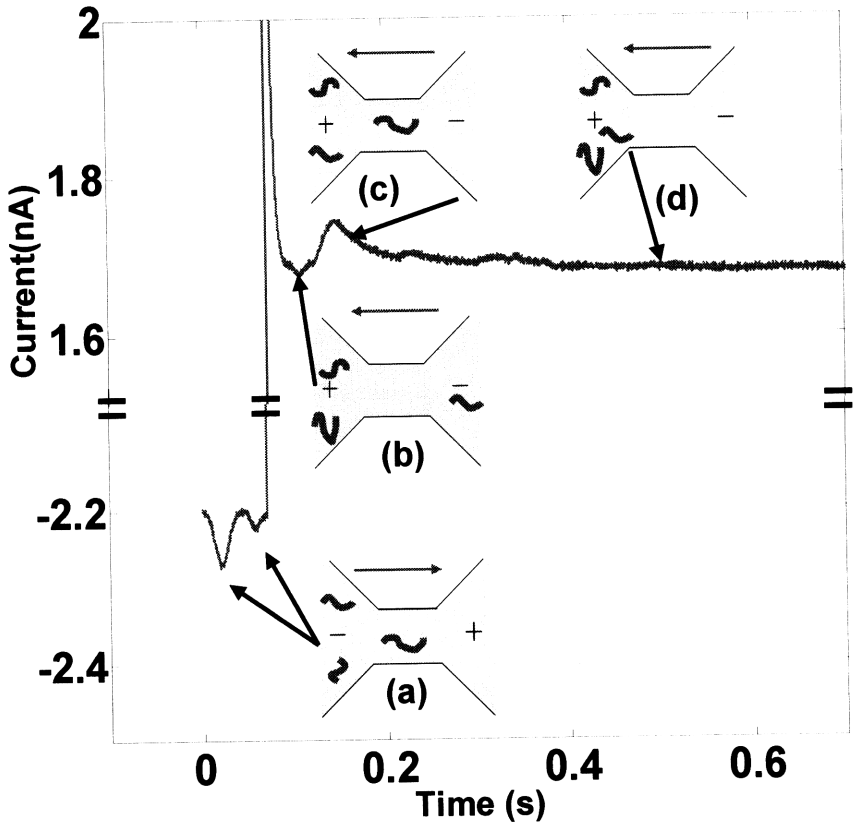

Figure 23 Multiple measurements with feedback control with a solution of 7.5 μg/mL DNA on the left side (10mM KCl, voltage bias ±1 V) in a nanopore of 200 nm × 500 nm × 5 μm (a) DNA traverses from left microchannel reservoir through the nanopore, triggering voltage reversal. Concentration polarization results in a transient current spike. (b) DNA now in the right microchannel reservoir; ionic current equals open-channel value. (c) The DNA molecule again traverses through the nanopore, and a translocation is detected. (d) DNA now in the left reservoir; ionic current goes back to open-channel value and no more translocation signals are detected.

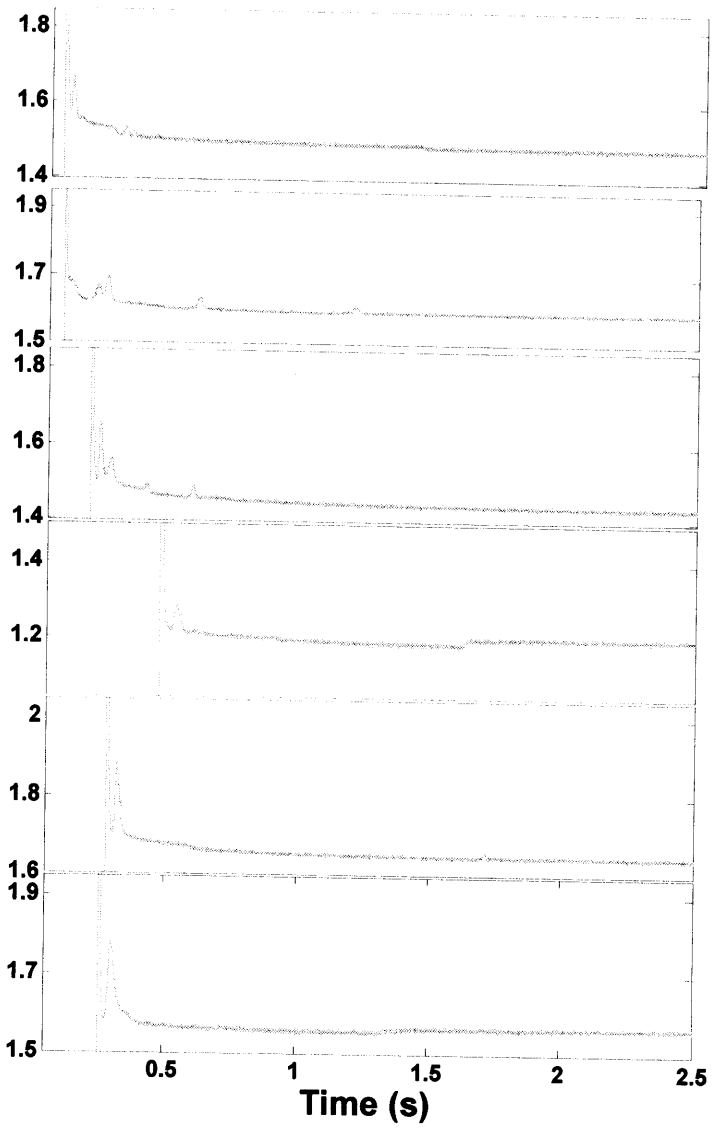

Figure 24 Other DNA translocation data showing the multiple events of successful recapture of DNA after voltage reversal.

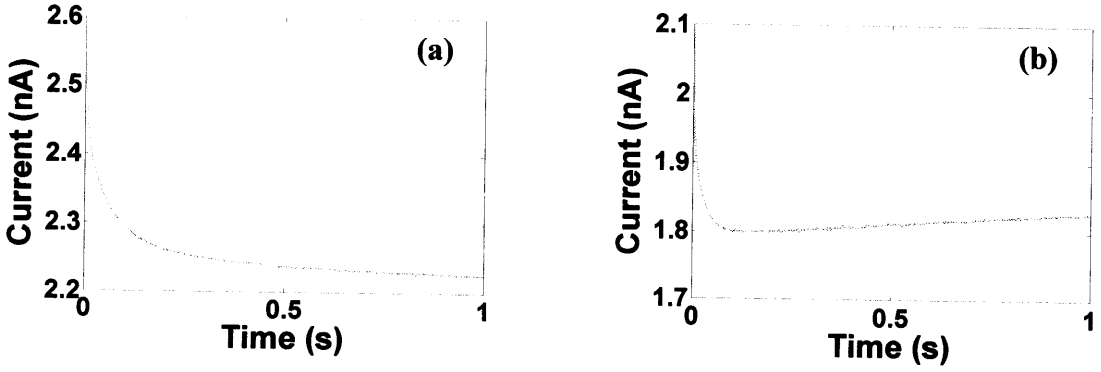

Figure 25 (a) Current value with 10 mM KCl buffer solution immediately after voltage reversal. Transient high current is observed due to concentration polarization. (b) Current observed upon voltage reversal with 10 mM KCl and 7.5 μg/mL λ-DNA on left side before any translocation signal was detected. Both experiments did not show DNA translocation signals after voltage reversal.

4.4 Discussion

It is shown from experimental data of figure 4 and 5 that multiple (two) measurements on the same molecule had been implemented in our system. However, several issues still need to be resolved in order to (1) recapture every single DNA molecule that has been translocated through the nanopore before being displaced by another DNA molecule, and (2) extend the number of measurements from two to >10. Below we describe approaches to address issues above.

(a) Decrease the concentration of analyte so that given the same magnitude of voltage bias, DNA translocation rate could be lowered significantly, which results in lower chances of having the trapped molecule that is supposed to be recaptured by the nanopore getting displaced by another molecule entering the pore.

(b) The delay between the escape of the DNA molecule and voltage reversal could be minimized by implementing the current measurement/comparison and data recording separately[44]. Specifically, we can implement the measurement and comparison algorithm using LabVIEW software installed in computer, and record the current data to disk using Digidata 1322A digitizer (Molecular Devices) and associated pClamp software (Molecular Devices).

(c) The recapture rate in our system was about 20%. Besides eliminating the time delay between the escape of molecule out of the nanopore and the voltage reversal, another approach involves fabrication of nanofluidic reservoirs that have smaller cross sectional area to ensure trapping of the analyte (Figure 19).

4.5 Conclusion

Here we have demonstrated a simple nanofluidic Coulter counter system with feedback control that enables two measurements on the same molecule of λ-DNA. The electronic hardware setup is the same as that used in measuring the translocation events of λ-DNA, and the software code is written in LabVIEW. Control studies confirmed that these events were due to λ-DNA translocating back through nanopore. This device is the first step towards nanoscale Coulter counter systems that can perform statistical averaging over multiple translocation events of the *same* molecule to greatly enhance the signal-to-noise ratio for sizing nanoscale analytes. Future work involves optimizing the concentration of analyte and the magnitude of voltage, measuring/comparing and recording current data separately, and fabrication of nanofluidic reservoirs on either side of the nanopore to ensure every DNA molecule to be recaptured before being displaced by another DNA molecule in order to extend the number of measurements from two to >10. If successful, this approach may lead to nanopore systems that far exceed the analytical capabilities of comparable systems with only one measurement per particle.

Chapter 5 Conclusion and Outlook

In this thesis we focused on characterizing and controlling the translocation of single 48.5 kbp λ-DNA molecule through an artificial PDMS nanopore with the objective of enabling *multiple* measurements on the same molecule. 48.5 kbp λ-DNA was chosen as analyte since it can be detected in relatively large nanopores. Soft-lithography was adopted because of its ease of fabrication and capability to fabricate nanofluidic reservoirs for trapping analyte.

Issues such as cleanness of the wafer, temperature and length for baking PDMS, cleanness of the PDMS device and glass slide were found to be critical factors for successfully fabricating a PDMS nanopore sensor device.

We successfully detected 48.5 kbp λ-DNA single molecules with our PDMS nanopore. Factors such as device stability, DNA translocation events and signal-to-noise ratio are critical to successful implementation of multiple measurements with feedback control. By coating the device with BSA, stability was greatly improved. Factors such as applied voltage bias, concentration of analyte, and dimensions of the channel were found to affect the frequency of translocation events and signal-to-noise ratio. Moreover, we characterized DNA translocation events, and found that DNA translocation events through the nanopore *after* the completion of previous DNA translocation were similar to the Poisson process. In addition, noise contributions from LabVIEW/Axopatch interface, the addition of BSA, and increase of KCl concentration were characterized. This characterization could help optimize further experiment to increase measurement sensitivity of the system, and to successfully implement multiple measurements with feedback control.

For the proof-of-concept toward multiple measurements on the same molecule, we have implemented two measurements on the same molecule in our system.

For multiple measurements on the same molecule, we encountered issues such as multiple molecules entering the nanopore at the same time, low recapture rate, and time lag between escape of molecule and voltage reversal. These issues could be solved by optimizing LabVIEW algorithm, optimizing the concentration of analyte and the magnitude of voltage, measuring/comparing and recording current data separately, and fabrication of nanofluidic reservoirs on either side of the nanopore to ensure every DNA molecule to be recaptured before being displaced by another DNA molecule. This approach could lead to the enhancement of measurement capability and signal-to-noise ratio.

Reference:

1. Ibrahim, S.F. & van den Engh, G. High-speed cell sorting: fundamentals and recent advances. *Curr Opin Biotech* **14**, 5-12 (2003).
2. Sohn, L.L. & Saleh, O.A. Direct detection of antibody-antigen binding using an on-chip artificial pore. *Proceedings of the National Academy of Sciences of the United States of America* **100**, 820-824 (2003).
3. Saleh, O.A. & Sohn, L.L. Binding assays and single molecule sensing using precision chip-based resistive sensing. *Biophysical Journal* **82**, 166a-166a (2002).
4. Saleh, O.A. & Sohn, L.L. Quantitative sensing of nanoscale colloids using a microchip Coulter counter. *Review of Scientific Instruments* **72**, 4449-4451 (2001).
5. Karhanek, M., Kemp, J.T., Pourmand, N., Davis, R.W. & Webb, C.D. Single DNA molecule detection using nanopipettes and nanoparticles. *Nano Letters* **5**, 403-407 (2005).
6. Kasianowicz, J.J., Brandin, E., Branton, D. & Deamer, D.W. Characterization of individual polynucleotide molecules using a membrane channel. *Proceedings of the National Academy of Sciences of the United States of America* **93**, 13770-13773 (1996).
7. Howorka, S. & Bayley, H. Probing distance and electrical potential within a protein pore with tethered DNA. *Biophysical Journal* **83**, 3202-3210 (2002).
8. Li, J. et al. Ion-beam sculpting at nanometre length scales. *Nature* **412**, 166-169 (2001).
9. Meller, A., Nivon, L. & Branton, D. Voltage-driven DNA translocations through a nanopore. *Physical Review Letters* **86**, 3435-3438 (2001).
10. Storm, A.J., Chen, J.H., Ling, X.S., Zandbergen, H.W. & Dekker, C. Fabrication of solid-state nanopores with single-nanometre precision. *Nature Materials* **2**, 537-540 (2003).
11. Bayley, H. & Martin, C.R. Resistive-pulse sensing - From microbes to molecules. *Chemical Reviews* **100**, 2575-2594 (2000).
12. Henriquez, R.R., Ito, T., Sun, L. & Crooks, R.M. The resurgence of Coulter counting for analyzing nanoscale objects. *Analyst* **129**, 478-482 (2004).
13. Meller, A., Nivon, L., Brandin, E., Golovchenko, J. & Branton, D. Rapid nanopore discrimination between single polynucleotide molecules. *Proceedings of the National Academy of Sciences of the United States of America* **97**, 1079-1084 (2000).
14. Chang, H. et al. DNA-mediated fluctuations in ionic current through silicon oxide nanopore channels. *Nano Lett* **4**, 1551-1556 (2004).
15. Smeets, R.M.M., Keyser, U.F., Dekker, N.H. & Dekker, C. Noise in solid-state nanopores. *Proceedings of the National Academy of Sciences of the United States of America* **105**, 417-421 (2008).
16. Saleh, O. & Sohn, L. An artificial nanopore for molecular sensing. *Nano Letters* **3**, 37-38 (2003).
17. Deamer, D.W., Akeson, M. Nanopores and nucleic acids: prospects for ultrarapid sequencing. *Trends in Biotech.* **18**, 147-151 (2000).

18. Kasianowicz, J.J. & Bezrukov, S.M. Protonation Dynamics of the Alpha-Toxin Ion-Channel from Spectral-Analysis of Ph-Dependent Current Fluctuations. *Biophysical Journal* **69**, 94-105 (1995).
19. Deamer, D.W., Akeson, M. Nanopores and nucleic acids: prospects for ultrarapid sequencing. *Trends in Biotech.* **18**, 147-151 (2000).
20. Bates, M., Burns, M. & Meller, A. Dynamics of DNA molecules in a membrane channel probed by active control techniques. *Biophysical Journal* **84**, 2366-2372 (2003).
21. Wang, H., Dunning, J.E., Huang, A.P.H., Nyamwanda, J.A. & Branton, D. DNA heterogeneity and phosphorylation unveiled by single-molecule electrophoresis. *Proceedings of the National Academy of Sciences of the United States of America* **101**, 13472-13477 (2004).
22. Smeets, R.M.M. et al. Salt dependence of ion transport and DNA translocation through solid-state nanopores. *Nano Lett* **6**, 89-95 (2006).
23. Siwy, Z. et al. Preparation of synthetic nanopores with transport properties analogous to biological channels. *Surf Sci* **532**, 1061-1066 (2003).
24. Siwy, Z. et al. Protein biosensors based on biofunctionalized conical gold nanotubes. *J Am Chem Soc* **127**, 5000-5001 (2005).
25. Harrell, C.C., Kohli, P., Siwy, Z. & Martin, C.R. DNA - Nanotube artificial ion channels. *J Am Chem Soc* **126**, 15646-15647 (2004).
26. Ito, T., Sun, L. & Crooks, R.M. Simultaneous determination of the size and surface charge of individual nanoparticles using a carbon nanotube-based coulter counter. *Analytical Chemistry* **75**, 2399-2406 (2003).
27. Deblois, R.W. & Wesley, R.K.A. Sizes and Concentrations of Several Type-C Oncornaviruses and Bacteriophage-T2 by Resistive-Pulse Technique. *J Virol* **23**, 227-233 (1977).
28. Carbonaro, A. & Sohn, L.L. A resistive-pulse sensor chip for multianalyte immunoassays. *Lab Chip* **5**, 1155-1160 (2005).
29. Karnik, R. et al. Electrostatic control of ions and molecules in nanofluidic transistors. *Nano Letters* **5**, 943-948 (2005).
30. Uram, J.D., Ke, K., Hunt, A.J. & Mayer, M. Submicrometer pore-based characterization and quantification of antibody-virus interactions. *Small* **2**, 967-972 (2006).
31. Uram, J.D., Ke, K., Hunt, A.J. & Mayer, M. Label-free affinity assays by rapid detection of immune complexes in submicrometer pores. *Angew Chem Int Edit* **45**, 2281-2285 (2006).
32. Stein, D., Kruithof, M. & Dekker, C. Surface-charge-governed ion transport in nanofluidic channels. *Physical Review Letters* **93**, - (2004).
33. Karnik, R., Castelino, K., Fan, R., Yang, P. & Majumdar, A. Effects of biological reactions and modifications on conductance of nanofluidic channels. *Nano Letters* **5**, 1638-1642 (2005).
34. Fan, R. et al. DNA translocation in inorganic nanotubes. *Nano Lett* **5**, 1633-1637 (2005).
35. Sigalov, G., Comer, J., Timp, G. & Aksmentiev, A. Detection of DNA sequences using an alternating electric field in a nanopore capacitor. *Nano Lett* **8**, 56-63 (2008).

36. Chen, P. et al. Atomic layer deposition to fine-tune the surface properties and diameters of fabricated nanopores. *Nano Letters* **4**, 1333-1337 (2004).
37. Trepagnier, E.H., Radenovic, A., Sivak, D., Geissler, P. & Liphardt, J. Controlling DNA capture and propagation through artificial nanopores. *Nano Lett* **7**, 2824-2830 (2007).
38. Siwy, Z. & Fulinski, A. Origin of 1/f(alpha) noise in membrane channel currents. *Phys Rev Lett* **89**, - (2002).
39. Smeets, R.M.M., Keyser, U.F., Wu, M.Y., Dekker, N.H. & Dekker, C. Nanobubbles in solid-state nanopores. *Phys Rev Lett* **97**, - (2006).
40. Tabard-Cossa, V., Trivedi, D., Wiggin, M., Jetha, N.N. & Marziali, A. Noise analysis and reduction in solid-state nanopores. *Nanotechnology* **18**, - (2007).
41. Uram, J.D., Ke, K. & Mayer, M. Noise and bandwidth of current recordings from submicrometer pores and nanopores. *Acs Nano* **2**, 857-872 (2008).
42. Saleh, O.A. & Sohn, L.L. Correcting off-axis effects in an on-chip resistive-pulse analyzer. *Review of Scientific Instruments* **73**, 4396-4398 (2002).
43. Drake, A.W. Fundamentals of applied probability theory. (McGraw-Hill, New York; 1967).
44. Gershow, M. & Golovchenko, J.A. Recapturing and trapping single molecules with a solid-state nanopore. *Nat Nanotechnol* **2**, 775-779 (2007).
45. Biance, A.L. et al. Focused ion beam sculpted membranes for nanoscience tooling. *Microelectron Eng* **83**, 1474-1477 (2006).
46. Kim, M.J., Wanunu, M., Bell, D.C. & Meller, A. Rapid fabrication of uniformly sized nanopores and nanopore arrays for parallel DNA analysis. *Adv Mater* **18**, 3149-+ (2006).
47. Zhang, J.M., You, L.P., Ye, H.Q. & Yu, D.P. Fabrication of ultrafine nanostructures with single-nanometre precision in a high-resolution transmission electron microscope. *Nanotechnology* **18**, - (2007).
48. Stein, D.M., McMullan, C.J., Li, J.L. & Golovchenko, J.A. Feedback-controlled ion beam sculpting apparatus. *Review of Scientific Instruments* **75**, 900-905 (2004).
49. Gierak, J. et al. Sub-5 nm FIB direct patterning of nanodevices. *Microelectron Eng* **84**, 779-783 (2007).
50. Siwy, Z., Dobrev, D., Neumann, R., Trautmann, C. & Voss, K. Electro-responsive asymmetric nanopores in polyimide with stable ion-current signal. *Appl Phys a-Mater* **76**, 781-785 (2003).
51. Apel, P.Y., Korchev, Y.E., Siwy, Z., Spohr, R. & Yoshida, M. Diode-like single-ion track membrane prepared by electro-stopping. *Nucl Instrum Meth B* **184**, 337-346 (2001).
52. Xia, Y.N. & Whitesides, G.M. Soft lithography. *Annu Rev Mater Sci* **28**, 153-184 (1998).
53. Daoudil, S.B., F. Flows of Flexible Polymer Solutions in Pores. *Macromolecules 11*, 751 - 758 (1978).
54. Huh, D. et al. Tuneable elastomeric nanochannels for nanofluidic manipulation. *Nature Materials* **6**, 424-428 (2007).

55. Duffy, D.C., McDonald, J.C., Schueller, O.J.A. & Whitesides, G.M. Rapid prototyping of microfluidic systems in poly(dimethylsiloxane). *Anal Chem* **70**, 4974-4984 (1998).
56. Travis, J., Kring,J. LabVIEW for Everyone. *Prentice Hall* (2006).
57. Han, J., Turner, S.W. & Craighead, H.G. Entropic trapping and escape of long DNA molecules at submicron size constriction. *Physical Review Letters* **83**, 1688-1691 (1999).
58. Stein, D. Nanopores - Molecular ping-pong. *Nat Nanotechnol* **2**, 741-742 (2007).
59. Cockroft, S.L., Chu, J., Amorin, M. & Ghadiri, M.R. A single-molecule nanopore device detects DNA polymerase activity with single-nucleotide resolution. *J Am Chem Soc* **130**, 818-+ (2008).